Chapter 2
Theory

In this chapter, we build the theoretical outline for understanding the fundamental electrodynamic and photophysical properties of a fluorescent emitter. We start with a quantum mechanical picture where we introduce a fluorescent molecule as a dipole emitter with a fixed transition dipole moment oriented in its molecular structure. Thereafter, we consider a dipole in an empty box with boundary conditions on the electromagnetic field's periodicity, in order to determine its absorption and emission coefficients and connect these properties with its spontaneous emission rates. In order to account for its emission properties in the presence of a dielectric or a metal interface, we introduce a dipole in a semi-classical quantum optical framework. We start from a basic description of plane waves using Maxwell's equations, Fresnel's equations for reflection and transmission, etc. and ultimately calculate the total radiation power of a dipole as a function of its distance and orientation from such an interface. This completes our introduction to the concept of Metal Induced Energy Transfer (MIET).

2.1 Quantum Mechanical Picture of Fluorescence

From a quantum mechanical viewpoint fluorescence is a process which involves a repeated transition of a molecule between two quantized energy states (or the transition of electrons between two molecular orbitals) given by wave functions, say ψ_1 and ψ_2. The excitation from the ground state to the excited state takes place following an absorption of a photon of energy $h\nu$, followed by the decay of the molecule from the excited state back to the ground state. This is achieved either by the emission of a photon, or non-radiatively by transferring the energy to the surroundings or lost internally. The excitation and de-excitation processes are accompanied by perturbations in the delocalized electron cloud over the molecule's framework. These perturbations depend on the probability of a transition between two energy states and also on the selection rules based on the symmetry of the structure of molecular orbitals involved. Therefore, each transition takes place along a preferred direction

N. Karedla, *Single-Molecule Metal-Induced Energy Transfer*,
Springer Theses, DOI 10.1007/978-3-319-60537-1_2

in the molecule's framework which is known as the *transition dipole moment*, and the magnitude of this vector represents the probability of this transition. Below, we will briefly introduce this concept and touch upon some fundamental photophysical properties of a fluorescent molecule that are otherwise hard to explain from a purely classical framework.

2.1.1 Molecular Excitation and Emission

A complete explanation for the electronic spectra of molecules is extremely complex. An electronic transition is coupled with vibrational and rotational transitions which makes it even more complicated. However, in this section we will state some general rules and fundamental principles associated with the excitation and emission phenomena of fluorescent dyes. We refrain ourselves from dealing with the detailed quantum chemical treatment of the molecular states (those who wish to dive into the ocean might start by referring to excellent books such as [1]). To begin with, the molecular states are treated as a linear combination of all the atomic orbitals involved, which acts as a good starting point for the molecular orbital theory. The wavefunction of a molecule in each state gives the overall probability of the electron's position in space.

Keeping the discussion between two nuclei and a single electron for the sake of simplicity, when two atomic orbitals ϕ_1 and ϕ_2 interact, two molecular orbitals $\psi_+ = \phi_1 + \phi_2$ and $\psi_- = \phi_1 - \phi_2$ are formed, where ψ_+ has lower energy, and is therefore called as *bonding orbital*, than ψ_-, which we call as an *antibonding orbital*. The potential energy curves, as a function of the internuclear distance, can be obtained by calculating the Hamiltonian over these wavefunctions. The potential energy depends on electron-nuclei interactions, the angular momentum of the electron's spin around its own axis and in the orbital, spin-orbital coupling, and other factors which play a major role in deciding the fate of the electron in each state. Figure 2.1 shows the general characteristics of potential energy observed for a bonding and antibonding orbital. Depending on the symmetry and shape of the atomic orbitals involved, the molecular orbitals can be singly (σ) or doubly degenerate (π). In a many electron system, the electron-electron repulsion plays a dominant role too. Due to these interactions, the electrons occupy the energy states starting from the lowest energy state following Hund's rule of maximum multiplicity for the electron spin and Pauli's exclusion principle. The Highest Occupied Molecular Orbital is called the HOMO and the Lowest Unoccupied Molecular Orbital, above the HOMO in the energy ladder is termed the LUMO. We must emphasize here that for many electron systems, the potential energy between two nuclei is the effective curve taking all the electrons in the bonding and the antibonding orbitals into consideration. Thus, the two nuclei will be driven apart, or the bond is broken only when the net curve has antibonding nature. In other words, one can see the net potential energy curve as a summation of the curves calculated for each electron individually in its respective molecular orbital. We follow the general naming of the molecular orbitals such as σ and σ^*, π and π^* for bonding and anti-bonding orbitals of degeneracy one and two respectively; and n and n^* for non-bonding molecular orbitals which

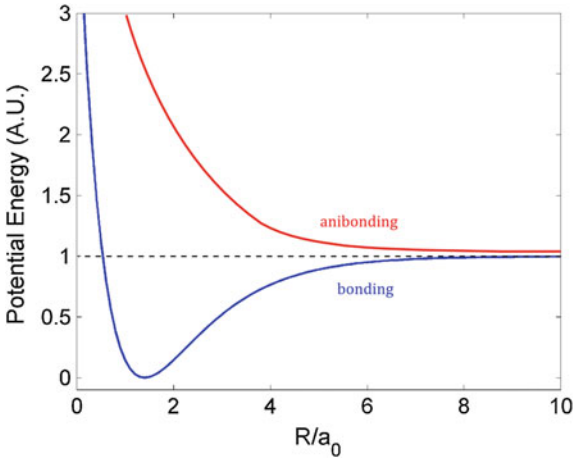

Fig. 2.1 An exemplary plot showing energy as a function of distance for a bonding and an antibonding orbital

constitute a lone pair of electrons from an atom which does not take part in bond formation. The electrons can undergo electronic transitions to the higher antibonding states upon interaction with an incident electromagnetic radiation, but in some cases these orbitals are orthogonal to all the participating atomic orbitals and thus also the molecular orbitals, thereby prohibiting any such transitions.

This picture can be extrapolated to a polyatomic organic molecule where each atom contributes to one or more atomic orbitals for bonding with its neighboring atoms. In such a molecule, several electronic transitions are possible from its filled orbitals to higher vacant orbitals. Each transition requires a particular wavelength which is equal to the energy gap between the two molecular orbitals, and have different probabilities. The absorption and emission spectra for most strong electronic transitions in organic molecules are usually related to a transition involving a group of atoms in the molecule's structure, which is called the *chromophore*. The most common chromophores involve carbonyl, nitro, nitroso groups, and carbon-carbon double bond systems. Chromophores with alternate double bonds are planar systems and have their π orbitals over the entire conjugation. The wavefunctions of the molecular orbitals can thus be approximated as waves with nodes at the edges of this box. The lowest orbital has no nodes in between the conjugation length and thus allows the maximum electron density between all the atoms. The number of nodes increase by one for each higher energy molecular orbital. These are called Hückel's molecular orbitals, named after Erich Hückel who calculated the molecular orbital picture for conjugated π organic molecules, including cyclic molecules. For a linear conjugated system with i number of π bonds, i molecular orbitals involved in the bonding. The energy of each state is given by $E_n = n^2h^2/8mL^2$, where L is the total length of the molecule (here one can approximate L as i times the length of a carbon-carbon bond with a bond order of 1.5) and m is the reduced mass of the electron. For such a molecular system, HOMO is the i^{th} molecular orbital and LUMO the $i + 1$th, and therefore the excitation wavelength ($\lambda = hc/(E_{i+1} - E_i)$), can be

calculated using the simple equation

$$\lambda = \frac{8mL^2c}{h(2i+1)} \tag{2.1}$$

For dye molecules that absorb and fluoresce in the visible range, mainly the transitions between $\pi \leftrightarrow \pi^*$ and $n \leftrightarrow \pi^*$ are responsible. Thus the shape of the frontier orbitals (HOMO and LUMO) is chiefly determined by the conjugation structure of the chromophore. The wavelength range for the transitions $\sigma \leftrightarrow \sigma^*$ usually lies in the ultraviolet region.

The complete absorption spectra of polyatomic chromophores contains all the transitions that are possible. Each transition is associated with two molecular orbitals, and therefore represents a change of electron density over the structure of the molecule along a particular direction termed the *transition dipole*. For a transition between two states with wavefunctions ψ_f and ψ_i, the associated *transition dipole moment* is defined as

$$\hat{\mathbf{M}}_{fi} = \left\langle \psi_f^* \left| q\hat{\mathbf{r}} \right| \psi_i \right\rangle = \int \psi_f^* \, q\hat{\mathbf{r}} \, \psi_i \, \mathrm{d}\tau \tag{2.2}$$

where $q\hat{\mathbf{r}}$ is the electric dipole moment operator and $\hat{\mathbf{M}}_{fi}$ is the matrix element of the transition dipole matrix $\hat{\mathbf{M}}$ corresponding to the transition $\psi_f \leftrightarrow \psi_i$. Clearly, the characteristics of ψ_i and ψ_f play an important role in determining the magnitude of the transition between the two states, which give us the selection rules that are fundamental for all spectroscopic studies. If the expectation value for the transition dipole moment operator between the two states is zero, the transition takes place infrequently and it is said to be *forbidden*, and if it is a finite value, it is called an *allowed* transition. Since the dipole operator is a translation operator $\hat{\mathbf{r}}$ times charge, it depends only on the spatial part of the wave functions. One can interpret this is in the following way: if the molecular orbital ψ_i overlaps in space with the molecular orbital ψ_f then the molecule will absorb energy from an EM radiation with energy equal to the energy gap between these two orbitals. However, exceptions exist. An example where this is not true, i.e. where the orbitals are spatially orthogonal, is a $\pi^* \leftarrow n$ transition in a carbonyl group. Since we already realized above that the non-bonding orbital n is orthogonal to all the molecular orbitals, the transition is forbidden. But, a weak absorbance is observed in most of the molecules containing the carbonyl group due to several reasons. One basic reason which we did not consider in all the arguments made above is the spin-orbital coupling which is beyond the scope of this thesis. It is strenuous to calculate the dipole moment of each transition for complicated structures such as for those shown in Fig. 2.2. But, simple rules from group theory in quantum mechanics can be of great help to predict at least which transition probabilities are necessarily zero or forbidden (see Chap. 11 from the book [2] for example).

The spectra of the chromophore group shift towards longer wavelengths due to the presence of other functional groups attached to it such as hydroxyl, amino, oxymethyl

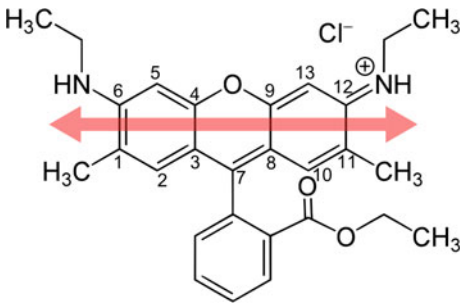

Fig. 2.2 The structure of Rhodamine 6G showing the orientation of the transition dipole moment. The carbon atoms of the Xanthene core atoms are numbered C1 to C13. Two ethylamine auxochromes are attached one each on the carbons C6 and C12 which participate in the conjugation with the help of their lone pair of electrons. The group attached on C7 lies perpendicular to the plane of the chromophore due to steric hindrance and does not take part in the conjugation. The π molecular orbitals lie perpendicular to the frontier orbitals of the chromophore (see [5])

groups, which are called *auxochromes*. These auxochromes do not absorb or emit light themselves but when present next to a chromophore, they increase the conjugation length due to their own lone pair of electrons. One needs to take the auxochromes into account too while calculating the frontier orbitals for the dye molecules, which can majorly contribute to the shape of these orbitals by varying the number and position of the nodal planes in the chromophore's structure. For example, the chromophore responsible for the absorption and emission properties of Rhodamine 6G is the Xanthene core and if we look at the frontier orbitals of this chromophore alone, then the transition should take place with the shift of electron density majorly along the direction of O↔C7 [3]. However, experiments and theoretical calculations for this dye suggest the transition dipole moment along the direction of C12↔C6 [4]. This is due to the presence of the two amino auxochromes, whose lone pair of electrons also participate in the conjugation.

2.1.2 Single-Singlet and Singlet-Triplet Transitions

Under the assumption that the coupling of the spin and orbital angular momentum is weak, we can separate the wavefunction of each molecular orbital into a spin and a spatial part.

$$\psi(\mathbf{r}_1\sigma_1, \mathbf{r}_2\sigma_2) = \Psi(\mathbf{r}_1, \mathbf{r}_2)\mathcal{X}(\sigma_1, \sigma_2). \tag{2.3}$$

where $\mathcal{X}(\sigma)$ can be written as a combination of $\alpha(\sigma)$ or $\beta(\sigma)$ depending upon the sign of the electron spin ($\uparrow$ or $\downarrow$) respectively. These functions are the eigenvalues of the Hermitian spin angular-momentum operator, and therefore are orthogonal. The ground state of the molecule is, in a majority of cases, a *singlet state*, where the spin of the electrons are paired, $S = 0$. The spin multiplicity for such a paired state is

$2S + 1 = 1$. The spin part of the wave function is given by

$$\mathcal{X}_i(\sigma_1, \sigma_2) = [\alpha(\sigma_1)\beta(\sigma_2) - \beta(\sigma_1)\alpha(\sigma 2)] \tag{2.4}$$

The antisymmetric function above on the right side is the *Pauli principle* which states that the total wave function of a system of electrons must be antisymmetric with respect to the interchange of any two electrons. If σ_1 and σ_2 are interchanged, the sign of the function becomes negative. This represents the fact that the probability to find two electrons with same spin close to each other is zero. For the excited state however, when one electron is promoted to a higher molecular orbital, the total spin can be 0 or 1. The state when $S = 0$ is again a singlet, and the spin wavefunction is given by the same Eq. (2.4). But, for the total wave function to be antisymmetric, the spatial part has to be symmetric. Therefore,

$$\psi_f(\mathbf{r}_1, \mathbf{r}_2) = \left[\psi_1(\mathbf{r}_1)\psi_2(\mathbf{r}_2) + \psi_2(\mathbf{r}_1)\psi_1(\mathbf{r}_2)\right]. \tag{2.5}$$

where ψ_1 is the spatial wavefunction of obital in the ground state and When the total spin $S = 1$, the spin multiplicity is 3. This can be explained by the three possibilities for the spins of the two electrons involved. In this case the three associated wavefunctions are given by

$$\mathcal{X}_f(\sigma_1, \sigma_2)(\sigma_1, \sigma_2) = \begin{cases} [\alpha(\sigma_1)\alpha(\sigma_2)] & \uparrow\uparrow \\ [\alpha(\sigma_1)\beta(\sigma_2) + \beta(\sigma_1)\alpha(\sigma_2)] & \uparrow\downarrow \\ [\beta(\sigma_2)\beta(\sigma_1)] & \downarrow\downarrow \end{cases}$$

As the spin part is symmetric, the spatial wavefunction takes up the antisymmetric nature in order to obey the Pauli principle.

$$\therefore \psi_f(\mathbf{r}_1, \mathbf{r}_2) = \left[\psi_1(\mathbf{r}_1)\psi_2(\mathbf{r}_2) - \psi_2(\mathbf{r}_1)\psi_1(\mathbf{r}_2)\right]. \tag{2.6}$$

The Hamiltonian is applied only on the spatial terms, which serves as a good approximation. With this approximation, we immediately conclude that the energies of three possibilities for the state $S = 1$ are equal. Thus, it is called a *triplet state*. Further, the energy of the triplet excited state is less than the energy of a singlet excited state. This holds true for any excited state. The diagram in Fig. 2.3 shows the depiction of the states involved.

The wavefunction $\psi(\mathbf{r}_1\sigma_1, \mathbf{r}_2\sigma_2)$ is said to be *even parity* if it does not change its sign when the sign of the coordinates are inverted and it is *odd parity* otherwise. Since the dipole operator $\mathbf{p} = q\hat{\mathbf{r}}$ changes the sign $r \rightarrow -r$, the integral (2.2) vanishes if both the wavefunctions ψ_i and ψ_f have the same parity. Thus, either of them must have an odd and the other an even parity for the transition to take place. The even and odd nature of a wavefunction must not be confused with its symmetry with respect to the interchange of electrons. Separating the spin and spatial parts of the integral, we have

$$\langle \psi_f^* \ |\mathbf{p}| \ \psi_i \rangle = \langle \mathcal{X}_f | \mathcal{X}_i \rangle \int \psi_f^* \, q \, \hat{\mathbf{r}} \, \psi_i \, \mathrm{d}^3 r \tag{2.7}$$

The spin term, $\langle \mathcal{X}_f | \mathcal{X}_i \rangle$ is non-zero only if the wavefunctions for both the states are identical. This is the first selection rule for electronic transitions, and it states that the spin state must not be altered in an electric dipole transition. This means that *singlet* state to *triplet* state transition is forbidden and vice versa. Thus, a molecule is excited from its singlet ground state S_0 to its singlet excited state S_1, which then returns to the ground state undergoing either spontaneous or stimulated emission. This cycle process must go on indefinitely, unless, as a rare event, the molecule undergoes what is known as *intersystem crossing*, and ends up in a metastable triplet state T_1. The probability of this transition depends primarily on the spin-orbital interaction where the triplet state 'mixes' with the pure singlet states so that a perturbed triplet state t_1 is formed [6].

$$\psi_{t_1} = \psi_{T_1} + \sum_k a_k \psi_{S_k} \tag{2.8}$$

where a_k give the coefficient of mixing with all possible singlet states S_k due to spin-orbital interactions. The square of these coefficients is proportional to the probability for a transition to the perturbed triplet state

$$P = \frac{2\pi}{3\hbar^2} \sum_{k,\, j=1\to 3} (\mathrm{S}_k \left| q\hat{\mathbf{r}} \right| T_1^j)^2 \tag{2.9}$$

The mean lifetime of the triplet state is inversely proportional to the probability of singlet-triplet transition [7]. For a typical organic fluorophore, this is around $10^{-6} \sim 10^{-4}\, s$. During this time, the excitation-emission fluorescence cycle is broken, and the dye remains in the dark state. This temporal intermittency of intensity from a dye molecule is known as *blinking*.

2.1.3 Franck-Condon Principle

When an electronic transition takes place, all the nuclei are assumed to be stationary. This treatment is similar to the Born-Oppenheimer approximation which relies on the fact that the nuclear masses are much larger than the electron mass and thus the motions of both can be separated. This is the *Franck-Condon principle* and is the basis of all the vibronic transition analysis following an electronic transition. Figure 2.3 illustrates the energy diagram of the transitions showing the vibrational states in each electronic state. The equilibrium positions in the higher electronic states are shifted towards larger distances due to the fact that they have higher antibonding character. When a transition takes place between S_0 and S_1, the internuclear distance is equal to the bond length in the ground state and since the nuclei motion are fixed, the transition occurs to the vibronic state where the internuclear distance is on

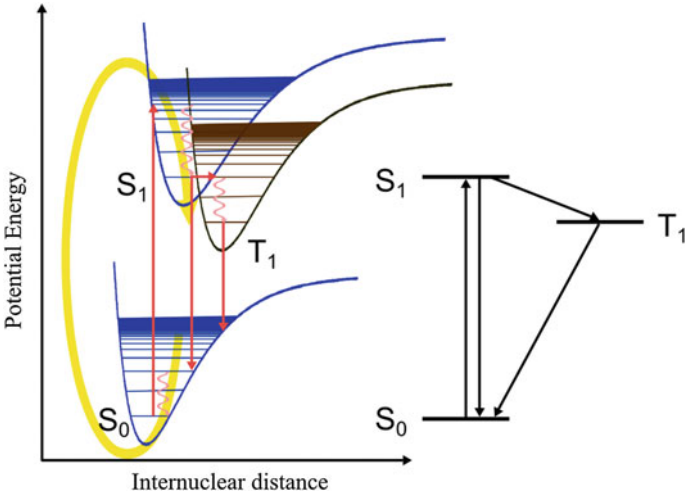

Fig. 2.3 Franck Condon diagram showing the potential energy curves for a singlet ground state and excited state (S_0 and S_1) and a triplet state T_1. The *red vertical arrows* show the vertical transitions from the ground state to excited states and back

the edge of the potential energy curve as shown in the figure. Such transitions are called *vertical transitions*. Thereafter, the nuclei vibrate at this energy level around the shifted equilibrium distance and readjust to the changes in the electron density which in-turn alters the overall electron density over the molecule, and so on until a new equilibrium state is attained. The same is observed when the transition takes place from the excited states to the ground state. The probability of transition is given by the square of the overlap integral between the two vibrational states in the respective electronic states.

$$F(\nu', \nu) = \left| \int \psi_\nu(\mathbf{R}) \psi^*_{\nu'}(\mathbf{R}) \, \mathrm{d}\tau_N \right|^2 \tag{2.10}$$

where ψ_ν and $\psi_{\nu'}$ are the wavefunctions of the vibronic states in the ground and the excited states respectively and $\mathbf{R}$ denotes the nuclear coordinates during the transition. At room temperature, the electronic transition usually proceeds from its ground vibronic level. The factors $F(\nu', \nu)$ are the Franck-Condon factors and contribute to the shape of the intensity spectrum of electronic transitions.

2.1.4 Radiationless De-Excitation

There are several relaxation processes in a molecule that proceed without the emission of photons. The *intersystem crossing*, where transitions occur between states of different multiplicity, introduced in the previous section, is an example. The relaxation of the molecule from higher excited states of the same multiplicity to the first

excited state (for example $S_n \rightarrow S_1$) non-radiatively is known as *internal conversion*. Radiative decay occurs with an appreciable yield only from the lowest excited state of a given multiplicity. This is the well-known *Kasha's rule* in photochemistry.

The radiationless relaxation of a molecule when excited to a higher state can be completely internal due to some rearrangement reactions in the excited state. As described briefly also in the previous section, an electronic excitation alters the nuclear coordinates and the electron density of the molecule. This structural change costs the molecule some energy which is called the *reorganization energy* (λ), and is an example of an ultrafast process which lasts about a few femtoseconds to picoseconds ($10^{-15} \sim 10^{-11}$s). A well-known example depicting this phenomenon is the phenolphthalein molecule in basic aqueous solutions (pH ~8.2 - 12). The phenolphthalein molecule, even though its structure is similar to the highly fluorescent fluorescein molecule, is non fluorescent. This is due to the fact that the total energy in its excited zero-order state (within the Born-Oppenheimer approximation) is converted into vibrational energy and torsional energy, which results in the rotation and vibration of the two phenyl rings attached to the central carbon. Whereas in the case of fluorescein, the two phenyl rings are fixed in a plane with two C-O bonds forming a rigid structure. In such a case, the rate of the non-radiative process is quenched and most of the relaxation takes place either radiatively or through intersystem crossing [8]. The rate of the intramolecular relaxations is related to λ, such that, for high values of λ (where the electronic and vibrational coupling is strong), the non-radiative rates are high [9]. The linewidth and the exponential decay of the non-radiative processes also depend on the interaction between the excited zero-order state and the density of all the vibronic states located close to that state [10], which, as one would expect, directly depends on the number of atoms in the molecule. This is straightforward if one writes the transition probability similar to Fermi's golden rule (see Eq. (2.19)). Due to the presence of 'sparse' energy levels in small molecules, no intramolecular electronic relaxation processes are encountered and relatively longer excited state lifetimes τ_f are observed [11].

In order to complete our discussion concerning the pathways of molecular emission, one must introduce the well-known property that is used to characterize a fluorescent emitter, the quantum yield of radiation (Φ). As the name suggests, it represents the probability an excited molecule decays radiatively. Quantitatively, it represents the ratio of the number of photons *emitted* by the molecule to the number of photons that the molecule absorbed in a given time. Given the radiative rate κ_r and the sum of all the non-radiative rates possible κ_{nr}, the quantum yield is defined as

$$\Phi = \frac{\kappa_r}{\kappa_r + \kappa_{nr}}. \tag{2.11}$$

2.1.5 Einstein's Coefficients and Spontaneous Emission Rate

In a seminal note from 1946 [12], Edward Mills Purcell first mentioned that it is possible to change the spontaneous emission rate of an emitter by placing it close to

a resonant structure, for example a metallic cavity. This change of the spontaneous emission rate is due to the action of the emitted field onto the emitter itself when it is back-scattered by the cavity. However, there is a deep connection between the spontaneous emission rate of a quantum-mechanical emitter and its absorption and stimulated emission coefficients: In thermal equilibrium, the number of photons per time absorbed by an emitter from the vacuum electromagnetic field has to be balanced by an equal number of photons per time emitted by that emitter. This imposes a rigid relation between absorption and emission properties of an emitter. In this section, we will briefly recall the connection between spontaneous emission rate and induced absorption and emission coefficients for an electric dipole emitter in empty space. Although this can be considered classical textbook knowledge, it will help us to define all relevant quantities which will be important in the following sections which considers the spontaneous emission rates of a dipole next to a dielectric or a metallic interface (Fig. 2.4).

We will start with considering an electric dipole emitter within an empty box of edge length L in thermal equilibrium at temperature T. It is assumed that the vacuum electromagnetic field within the box is in thermal equilibrium and obeys periodic boundary conditions with respect to the box. The vacuum electric field can be expanded into plane wave modes, $\mathbf{E} = \mathbf{E}_0 \exp(i\mathbf{k}\cdot\mathbf{r} - i\,\omega\,t)$, where $\mathbf{E}_0$ is the amplitude vector of a given mode and $\mathbf{k}$ its wave vector with length $k = \omega/\mathrm{c}$. Here, ω is the oscillation angular frequency of the mode, and c the vacuum speed of light, and is related to the frequency $\nu = \omega/2\pi$. The imposed boundary conditions imply that we have for the x-component of the wave vector $k_x L = 2\pi n_x$, where n_x is an integer number. Similar conditions hold also for the y- and z-components. Thus, the

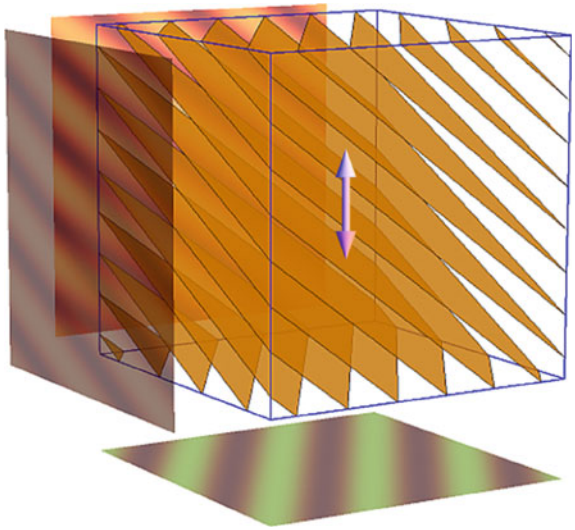

Fig. 2.4 A dipole situated in an empty cubic box with edge length L. The wavefronts of one plane wave mode and its phase on the three sides of the cubes are shown here

mode density ρ_ν within frequency interval $d\nu$ and solid angle element $\sin\theta \mathrm{d}\theta\mathrm{d}\phi$ is given by

$$\rho_\nu L^3 \mathrm{d}\nu \sin\theta \mathrm{d}\theta\mathrm{d}\phi = 2\frac{k^2 \mathrm{d}k \sin\theta \mathrm{d}\theta\mathrm{d}\phi}{(2\pi/L)^3} \tag{2.12}$$

where the factor 2 on the right hand side takes into account that there are two different principal polarisations of the electric field. Using Planck's energy quantization and Bose-Einstein statistics, the average energy per mode is

$$\epsilon_\nu = \frac{h\nu}{\exp(h\nu/k_B T) - 1} \tag{2.13}$$

where h is Planck's constant, k_B is Boltzmann's constant, and T is the temperature. Thus, when taking into account that the mean energy density (energy per unit volume) is ϵ_ν / L^3, one finds the mean energy density per solid angle and frequency to be equal to

$$\epsilon_\nu \rho_\nu \mathrm{d}\nu = 2\frac{k^2 \mathrm{d}k \sin\theta \mathrm{d}\theta\mathrm{d}\phi}{(2\pi/L)^3}\frac{1}{L^3}\frac{h\nu}{\exp(h\nu/k_B T) - 1} = \frac{2h\nu^3}{c^3}\frac{\mathrm{d}\nu \sin\theta \mathrm{d}\theta\mathrm{d}\phi}{\exp(h\nu/k_B T) - 1} \tag{2.14}$$

which is Planck's famous formula for black-body radiation.

Now, the mean energy absorbed by an electric dipole is proportional to this energy density times an orientation factor, integrated over all possible propagation directions. The orientation factor takes into account that only electric field components along the orientation of the emitter's dipole contribute to energy absorption, and it is given by $\langle|\hat{\mathbf{E}} \cdot \hat{\mathbf{p}}|^2\rangle = (1/2)\sin^2\theta$, where $\mathbf{p}$ is the electric dipole amplitude vector of the emitter which is assumed to be oriented along $\theta = 0$. The angular brackets denote averaging over all possible orientations of $\hat{\mathbf{E}}$ with $\hat{\mathbf{E}} \perp \mathbf{k}$. Thus, one finds the following expression for the mean density per frequency of the electromagnetic field which takes part in energy absorption by the dipole emitter

$$\begin{aligned} S(\nu)\mathrm{d}\nu &= \frac{h\nu^3}{c^3}\frac{\mathrm{d}\nu}{\exp(h\nu/k_B T) - 1}\int_0^{2\pi}\mathrm{d}\phi\int_0^{\pi}\sin\theta\cdot\sin^2\theta\mathrm{d}\theta \\ &= \frac{8\pi h\nu^3}{3c^3}\frac{1}{\exp(h\nu/k_B T) - 1} \end{aligned} \tag{2.15}$$

Considering all possible dipole orientations gives an additional factor of 3, and therefore, one has

$$S(\nu)\mathrm{d}\nu = \frac{8\pi h\nu^3}{c^3}\frac{1}{\exp\left(h\nu/k_BT\right)-1} \tag{2.16}$$

The *effective* mode density or Density of States (DOS) $\tilde{\rho}_\nu$ of the electromagnetic field that is coupled to the energy absorption by the dipole emitter is given by

$$\tilde{\rho}_\nu = \frac{8\pi\nu^2}{c^3} \tag{2.17}$$

From time dependent perturbation theory, the probability P for a transition of the molecular system between two quantum states with energies $\mathcal{E}_i$ and $\mathcal{E}_f$ when subjected to an electromagnetic radiation with an oscillation frequency ν for a time t_1, involving only the first order perturbation, averaged over all orientations of the dipole momemt $\mathbf{p}$ is given by [2]

$$P_{if}(t_1) = \frac{1}{3\hbar^2}|\mathbf{p}|^2 t_1 \int S(\nu)\left(\frac{\sin\frac{1}{2}(\nu_{if}-\nu)}{\frac{1}{2}(\nu_{if}-\nu)}\right)^2 \mathrm{d}\nu \tag{2.18}$$

where $\nu_{if} = |\mathcal{E}_f - \mathcal{E}_i|/h$. This shows that the transition probability has a sharp maximum when $\nu = \nu_{if}$ and other frequencies do not contribute much. Therefore, the transition probability per unit time, or *transition rate* between the two states is given by the expression

$$W_{f\leftarrow i} = \frac{2\pi|\mathbf{p}|^2 S(\nu_{if})}{3\hbar^2} \tag{2.19}$$

This is the well-known *Fermi's Golden Rule* for the transition probability between two states, which was originally derived by Paul Dirac in the year 1927 in his beautiful manuscript titled "The Quantum Theory of the Emission and Absorption of Radiation" [13]. The interesting point to realize from the equation above is that while $(\mathcal{E}_f - \mathcal{E}_i) = h\nu_{if}$ represents the *absorption* of the radiation incident on the molecule, the case where $(\mathcal{E}_i - \mathcal{E}_f) = -h\nu_{if}$ represents the case where a molecule present in the excited state falls into the state with lower energy, emitting radiation at the same frequency ν_{if}. This phenomenon is called *stimulated emission*. The expression for the transition probability for the stimulated emission can be written similar to the expression given in Eq. (2.18) by replacing ν_{if} with $-\nu_{if}$ which gives the same transition rate as in expression (2.19). Ignoring all higher orders of perturbation, at thermal equilibrium, the transition rate shown in equation (2.19) directly gives the *Einstein coefficient of stimulated absorption* B_{if}

$$W_{f\leftarrow i} = \frac{2\pi|\mathbf{p}|^2}{3\hbar^2}S(\nu_{if}) = B_{fi}S(\nu_{if}) \tag{2.20}$$

Since the transition rate for the stimulated emission is identical to the rate of stimulated absorption, the *Einstein coefficient of stimulated emission* B_{fi} is exactly the

same as B_{if}. Physically this translates to the statement that the same electromagnetic field which can excite the molecule from a state with lower energy to higher energy, can also act as an energy sink which brings the molecule from a higher energy state to a lower energy state. Therefore, one would conclude that the probability of finding a molecule in its ground state or excited state is equal. However, at a temperature T, if an ensemble of molecules is in thermal and radiation equilibrium the ratio of the population in the excited state to the ground state is given by Boltzmann statistics $\exp(-h\nu_{if}/k_BT)$. This supports the fact that a molecule in the excited state also emits radiation spontaneously, whether or not an external electromagnetic radiation field is present. Therefore, at equilibrium, one must have (Fig. 2.5)

$$N_f(A_{fi} + B_{fi}S(\nu_{if})) = N_i B_{if} S(\nu_{if}), \tag{2.21}$$

where N_i and N_f are the number of molecules in the initial and final state, respectively. A_{fi} in the equation above is the *Einstein coefficient of spontaneous emission*. From this equation the density of states $S(\nu_{if})$ can be written as

$$S(\nu_{if}) = \frac{\left[\frac{A_{fi}}{B_{fi}}\right]}{\left[\frac{B_{if}}{B_{fi}}\right]\left[\frac{N_i}{N_f}\right] - 1} \tag{2.22}$$

$$\because \frac{N_i}{N_f} = \exp\left(\frac{h\nu_{if}}{k_BT}\right) \text{ and } B_{if} = B_{fi}, \qquad S(\nu_{if}) = \frac{\left[\frac{A_{fi}}{B_{if}}\right]}{\exp\left(\frac{h\nu_{if}}{k_BT}\right) - 1} \tag{2.23}$$

Comparing with equation (2.16) one has

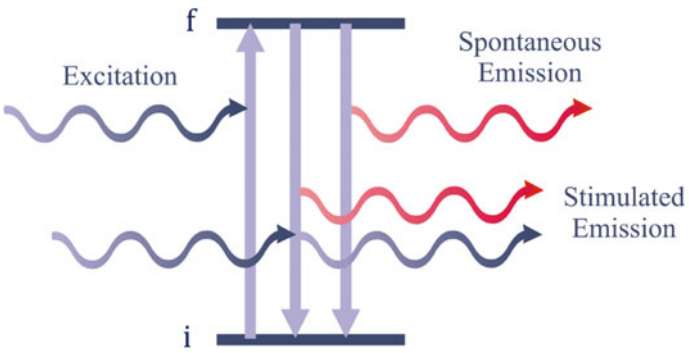

Fig. 2.5 Diagram illustrating the elementary transitions of a molecule between the two states i and f in Einstein's model

$$A_{fi} = \frac{8\pi h\nu_{if}^3}{c^3} B_{fi} = \tilde{\rho}_\nu h\nu B_{fi} \tag{2.24}$$

This shows that the spontaneous emission is proportional to the cube of the transition frequency ν_{if}. Also important to note here is that the spontaneous emission is directly related to the probability of absorption which is itself proportional to the square of the transition dipole moment, thus the *strength* of the dipole transition.

Note that three important fields of theories have been combined together here, namely Planck's theory for black body radiation, thermodynamics (Boltzmann distribution) and time dependent perturbation theory. The electromagnetic field here is also quantized and is seen as a collection of harmonic oscillators. The transfer of energy between the energy states of the radiation and the molecular system leads to the excitation and emission processes. The total rate of emission depends on both, the spontaneous emission and the stimulated emission. The mean lifetime of the molecule's exited state is inversely proportional to this total rate.

2.1.5.1 Absorption and Emission Cross Sections and Fluorescence Lifetimes

Let us for now model a molecule as a two state system, where there is no degeneracy associated with any of the states. The absorption cross section of a molecule, $\sigma_a(\nu)$, is the measure of the probability that it absorbs energy from the electromagnetic radiation field incident on it. It provides a relationship between the optical density of the sample and its concentration in spectroscopic analysis. It has the dimension of an area which can be interpreted as an effective cross-sectional area responsible for blocking an incident beam of electromagnetic waves of frequency ν. Let us define the stimulated absorption rate as

$$w_{i\to f}(\nu)\mathrm{d}\nu = b_{if}(\nu)S(\nu)\mathrm{d}\nu \tag{2.25}$$

where $S(\nu)$ is the energy density of the electromagnetic field per unit frequency and therefore $S(\nu)\mathrm{d}\nu$ is the energy density for the frequency range ν to $\nu + \mathrm{d}\nu$. $b_{if}(\nu)$ is the shape factor for the absorption spectrum of the molecule and represents the probability for the absorption at frequency ν to take place. The total rate of absorption is then the integral of the expression above.

$$W_{i\to f} = \int b_{if}(\nu)S(\nu)\mathrm{d}\nu \tag{2.26}$$

The absorption coefficient can be written in terms of direct measurable quantities, and it is simply the ratio of the total energy absorbed in unit time with the total incident irradiance I ($I = c\int S(\nu)\mathrm{d}\nu$).

$$\sigma_a(\nu) = \frac{h\nu W_{i\to f}}{I} = \frac{h\nu \int b_{if}(\nu)S(\nu)\mathrm{d}\nu}{c\int S(\nu)\mathrm{d}(\nu)} \tag{2.27}$$

If the absorption spectrum is approximated to a line spectrum, b_{if} is sharply peaked at ν_{fi} and is equal to B_{fi}, and hence, the absorption cross section can be written as

$$\sigma_a = \frac{h\nu_{fi}}{c} B_{if} \tag{2.28}$$

In a similar way, the emission cross section of the molecule can be written in terms of the emission coefficients

$$\sigma_e(\nu) = \frac{h\nu}{c} b_{fi}(\nu) = \frac{c^2}{8\pi\nu^2} a_{fi}(\nu) \tag{2.29}$$

The coefficient $a_{fi}(\nu)$ is the probability for the molecule in the excited state to decay spontaneously. Again, for the case of a sharp line spectrum, this is equal to A_{fi}. An important thing to mention here is that since the emission and absorption for such a two state system take place at the same frequency, the emission and absorption cross sections are completely identical $\sigma_e = \sigma_a \equiv \sigma$. In that case, the spontaneous decay lifetime τ_f, i.e. the statistical mean time the molecule stays in the excited state when there is no perturbation field is inversely proportional to the spontaneous emission coefficient A_{fi}, or,

$$\frac{1}{\tau_f} = \frac{8\pi}{c^2} \int \sigma(\nu)\nu^2 \mathrm{d}\nu = 8\pi c \int \frac{\sigma(\lambda)}{\lambda^4} \mathrm{d}\lambda \tag{2.30}$$

The above equation is known as the *Füchtbauer-Ladenburg relationship* [14] and it gives us the means to obtain the *radiative lifetime* of a two state system from the measured absorption/emission spectrum. This model works as a good approximation for the estimation of radiative rates of atomic transitions where the absorption and the emission take place at the same frequency that can be considered as sharp lines. See references [15, 16] for example. However, this theory fails to predict the transition rates for molecular systems accurately. The main reason for this deviation is that the spectra of the molecules are much broader due to the presence of vibrational and rotational energy levels within each electronic state. We shall discuss this aspect further in the next session. But for now, this can be visualized as a collection of many individual oscillators oscillating at slightly different frequencies that can interact with the electromagnetic field and have different transition probabilities. Moreover, the emission spectrum of a molecule is spectrally red shifted compared to its excitation spectrum. This is the well known *Stokes shift* of a fluorescent molecule.

In order to include this effect, Strickler and Berg modified the theory by taking into account all the vibrational quantum states [17]. The net transition rate is taken as the sum of the transition rates from the lowest vibrational level of the higher electronic state to all the possible vibrational levels of the ground state.

$$A_{f0\to i} = K \frac{8\pi h}{c^3} \frac{\sum_l \nu^3_{k0\to nl} b_{k0\to nl}}{\sum_l b_{k0\to nl}} \tag{2.31}$$

where the summations are performed over all the vibrational states l of the ground electronic state, and K is a proportionality constant. Each term in the numerator is proportional to the intensity in the emission spectrum. Hence, the total rate of spontaneous decay is written, similar to Eq. (2.30) in the integral form, as

$$\frac{1}{\tau_f} = \frac{8\pi}{c^2} \frac{\int \mathrm{d}\nu\, F(\nu)}{\int \mathrm{d}\nu\, F(\nu)/\nu^3} \int \mathrm{d}\nu\, \sigma_a(\nu)/\nu \tag{2.32}$$

where $F(\nu)$ are the Franck-Condon factors introduced previously, which shape the emission spectrum and the integral on the right is over the absorption spectrum of the molecule. This is the well-known *Strickler-Berg equation* which connects both the absorption and emission spectra for determining the average lifetimes of the molecules in their excited states. One must observe that as a special case, if the absorption and emission spectra are sharp and take place at the same frequency, this equation gives the same result as the Füchtbauer-Ladenburg relationship (2.30) shown above. The integral on the right side can be written in terms of experimentally measured molar extinction coefficients $\epsilon(\nu)$. Given the quantum yield of the molecule and the refractive index of the medium, the Strickler-Berg equation can be written as

$$\frac{1}{\tau_f} = 2.88 \times 10^{-9} n^2 \Phi \frac{\int \mathrm{d}\nu\, F(\nu)}{\int \mathrm{d}\nu\, F(\nu)/\nu^3} \int \mathrm{d}\nu\, \frac{\epsilon(\nu)}{\nu} \tag{2.33}$$

where ν is now the wavenumber in cm^{-1}. Figure 2.6 shows the spectra for the dye molecules Rhodamine 6G and Atto 655. The data for Rhodamine 6G has been taken from [18] and for Atto 655, from the website.[1] The quantum yields of these dyes are reported as 0.95 and 0.33 in the medium of the measurements. The spontaneous lifetimes calculated from Eq. (2.33) are 3.64 ns and 1.72 ns in water, whereas the true values reported in literature are 4.1 ns and 1.8 ns, respectively [19].

2.1.5.2 Spontaneous Emission Near Interfaces

In the preceding section we showed the connection between the spontaneous emission rate of a dipole emitter in empty space and the DOS $\tilde{\rho}_\nu$. When a molecule is present in a dielectric medium, the local DOS (LDOS) changes due to the scattering from the medium which leads to a modification of the spontaneous emission rates. Depending upon the solvent properties, thermal coupling between the dipole emitter and surrounding molecules can play a role in non-radiative energy transfer, due to collisions, known as *thermal decay* and hence shortening the lifetime of the molecule in the excited state [20].

The situation becomes complicated when placing such an emitter close to a dielectric or metallic interface. In that case, the spontaneous emission rate A_{fi} will change

[1] http://www.atto-tec.com/.

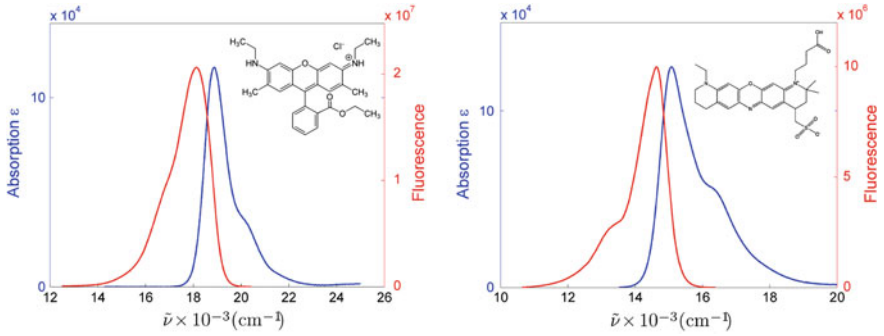

Fig. 2.6 The *left* figure shows the excitation/emission spectra of Rhodamine 6G in ethanol and the *right* side for Atto 655 in water. The plots are against wavenumbers $\tilde{\nu} = 1/\lambda$

and becomes position- *and* orientation-dependent. Also, the effective DOS will now be position- *and* orientation-dependent. One needs to calculate the LDOS in such a situation and use the relations developed in the previous section. The relation between the Einstein coefficients and LDOS remain the same as in Eq. (2.24). The properties of the metal determine the LDOS and depending on the distance from the metal, the electromagnetic coupling between the states of the dye molecule and the metal's surface plasmons varies, which together determine its radiative and non-radiative rates [21, 22]. However, the calculation of spontaneous emission rate of a dipole emitter is much more straightforward using the theory by Chance, Prock, and Silbey (CPS) where one calculates the total emission rates by using Fresnel's equations and energy *flux* density calculations using the Poynting vector [23]. This will the discussed thoroughly in the forthcoming sections.

2.2 Plane Waves and Maxwell's Equations

We begin our theoretical outline by highlighting the work of James Clerk Maxwell who set the groundwork for the electromagnetic theory of light in 1864. In classical electrodynamics, light is described as an electromagnetic wave (EM wave) with synchronized oscillations of electric (**E**) and magnetic (**B**) fields oriented orthogonal to each other, traveling with a speed c/n_{med} along a propagation direction **k**, where n_{med} is the refractive index of the medium, as shown in Fig. 2.7. By synchronized oscillations, we mean that the fields **E** and **B** have the same oscillation frequency and phase. The vector **k** is orthogonal to both **E** and **B**. The classical theory of light is based on the well known Maxwell's equations, which are the fundamental equations for electricity and magnetism. In CGS units, these equations can be written as

$$\nabla \cdot \epsilon \mathbf{E} = 4\pi \rho \tag{2.34}$$

$$\nabla \cdot \mathbf{B} = 0 \tag{2.35}$$

$$\nabla \times \mathbf{E} = -\frac{1}{c}\frac{\partial \mathbf{B}}{\partial t} \tag{2.36}$$

$$\nabla \times \left(\frac{\mathbf{B}}{\mu}\right) = \frac{\epsilon}{c}\frac{\partial \mathbf{E}}{\partial t} + \frac{4\pi}{c}\mathbf{j} \tag{2.37}$$

where ρ and $\mathbf{j}$ are the electric charge and current density respectively, and ϵ and μ are the dielectric susceptibility and magnetic permeability of the medium. These four equations were obtained from the well-known laws for electric and magnetic fields, the first two equations are Gauss' law for electric and magnetic fields; the third equation represents Faraday's law of magnetic induction and the fourth equation is Ampere's circuital law. These four coupled differential equations are satisfied simultaneously for all possible electromagnetic fields.

Equations (2.34) and (2.35) stem from the fact that electric charges can exist in space whereas magnetic monopoles do not; and the electric field exiting a volume is proportional to the charge density present inside it whereas the total flux of the magnetic field through a closed surface is always zero. Gauss' law holds true even for moving charges which makes it more general than Coloumb's law. The force due to an electromagnetic field on a charge particle moving with an arbitrary velocity $\mathbf{v}$ is given by the Lorentz force,

$$\mathbf{F} = q[\mathbf{E} + (\mathbf{v} \times \mathbf{B})]. \tag{2.38}$$

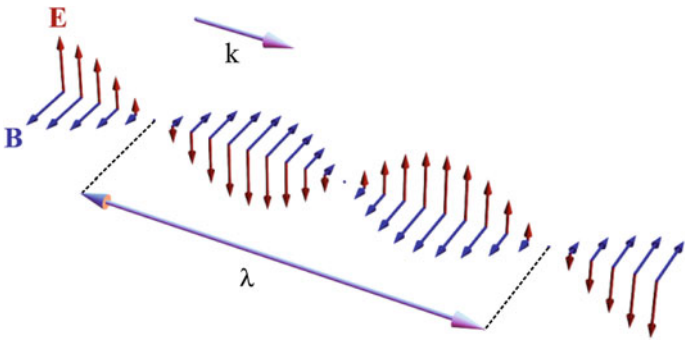

Fig. 2.7 A Schematic showing an electromagnetic wave at a time t with $\mathbf{E}$ and $\mathbf{B}$ oscillating orthogonal to the direction of propagation $\mathbf{k}$. The wavelength λ of the EM wave is marked here as the distance over one complete cycle of oscillation

An important point to note from Eq. (2.38) is that magnetic field due to any configuration of moving or static electric charges is always perpendicular to the direction of motion, and thus, does not perform any work.

In a source-free homogeneous medium with unity magnetic permeability $\mu = 1$ (which is true for all of the work in this thesis), the simplest solution to Maxwell's equations is a plane wave, where the space-time behavior of the electric (**E**) and magnetic (**B**) fields can be written as $\propto \exp(i\mathbf{k}\cdot\mathbf{r} - i\omega t)$, where ω is the angular frequency of the oscillations. Inserting this space-time relation back into the equations (2.34), (2.35), (2.36) and (2.37) we get

$$\mathbf{k}\cdot\mathbf{E} = 0 \tag{2.39}$$

$$\mathbf{k}\cdot\mathbf{B} = 0 \tag{2.40}$$

$$i\mathbf{k}\times\mathbf{E} = \frac{i\omega}{c}\mathbf{B} \tag{2.41}$$

$$i\mathbf{k}\times\mathbf{B} = -\frac{i\epsilon\omega}{c}\mathbf{E} \tag{2.42}$$

From equations (2.39) and (2.40), it is clear that **E**, **B** and **k** are mutually perpendicular. If we now apply the curl operator again on Eq. (2.36) and use the relations in equations (2.39) and (2.42), we obtain

$$\nabla\times\nabla\times\mathbf{E} = -\mathbf{k}\times(\mathbf{k}\times\mathbf{E}) = k^2\mathbf{E} = -\frac{\omega}{c}(\mathbf{k}\times\mathbf{B}) = \frac{\epsilon\,\omega^2}{c^2}\mathbf{E} \tag{2.43}$$

Therefore, from Eq. (2.43) we obtain the amplitude of the wave vector $|\mathbf{k}| = \sqrt{\epsilon}\,\omega/c$. The vector $|\mathbf{k}|$ characterizes the spatial periodicity of the electric field. If we define the refractive index of the medium by $n_{\text{med}} = \sqrt{\epsilon}$, we get the dispersion relation $|\mathbf{k}| = n_{\text{med}}\,\omega/c$ and the relation between the amplitudes of the electric and magnetic fields as $|\mathbf{B}| = n_{\text{med}}\,|\mathbf{E}|$.

For any electromagnetic field, the instantaneous energy flux is given by the Poynting vector **S**.

$$\mathbf{S} = \frac{c}{4\pi}\mathbf{E}\times\mathbf{B} \tag{2.44}$$

For visible light **S** oscillates with a frequency $\sim 10^{15}$ Hz, which cannot be measured with any instrument. What is measurable is the time-averaged energy flux density $\langle\mathbf{S}\rangle$ (averaged over one period of oscillation) for an electromagnetic field, which is

given by[2]

$$\langle \mathbf{S} \rangle = \frac{c}{8\pi} \mathrm{Re}\{\mathbf{E} \times \mathbf{B}^*\} \tag{2.45}$$

These relations hold true for any plane wave solution of the electromagnetic field in a source-free homogeneous environment. Further, any field in such an environment can be described as a superposition of plane waves. We will use these relations extensively in our forthcoming sections where we investigate the field of an oscillating electric dipole in such environments.

The interaction of EM waves with conducting media can be understood well with the help of the Drude model for conductivity. The model is based on the fact that the valence and the conduction bands of metals overlap at room temperature, and as a result a large number of free electrons exist that are responsible for their high conductivity. Therefore, any electromagnetic oscillations incident on a metal perturb the electrons on the surface which are then set into an oscillation with the same frequency in order to counter these perturbations. The existence of conductivity can be taken into account by simply introducing a complex dielectric constant into Maxwell's equations. The real of the dielectric constant (ϵ') is related to the bounded electrons and the lattice structure of the metal, whereas the imaginary part arises due to the free electrons. If we define σ as the specific conductivity of the material, then the *convection* current density $\mathbf{j}$ is given by

$$\mathbf{j} = \sigma \mathbf{E} \tag{2.46}$$

Note here that σ is a function of frequency since we saw that bound electrons can be excited into the conduction band. Plugging Eq. (2.46) into Maxwell's equation (2.37), we have

$$\boldsymbol{\nabla} \times \mathbf{B} = -\frac{i\,\omega}{c} \left[\epsilon'(\omega) + \frac{4\pi i}{\omega} \sigma(\omega) \right] \mathbf{E} \tag{2.47}$$

Using Eq. (2.43) we get the dispersion relation

$$k^2 = k_0^2 \left[\epsilon'(\omega) + \frac{4\pi i}{\omega} \sigma(\omega) \right] \tag{2.48}$$

where $k_0 = \omega/c$. The refractive index is thus a complex number which can be written as $\tilde{n} = n(\omega) + i\kappa(\omega)$.

$$\therefore \quad \tilde{n}^2(\omega) = [n(\omega) + i\kappa(\omega)]^2 = \epsilon'(\omega) + \frac{4\pi i}{\omega} \sigma(\omega) = \epsilon(\omega) \tag{2.49}$$

This brings us to the relations

[2]For derivation refer to "Principles of Optics", Born and Wolf [24].

$$\epsilon' = n^2 - \kappa^2 \tag{2.50}$$

and,

$$\frac{2\,\pi\,\sigma}{\omega} = n\kappa \tag{2.51}$$

2.3 Fresnel's Equations

After having familiarized ourselves with the basic properties of plane waves in a homogeneous environment, we now study their behavior when they encounter a locally flat interface separating two homogeneous media with different refractive indices n_1 and n_2. The wave vector $\mathbf{k}$ again represents a plane wave with a spatial periodicity of $|\mathbf{k}|$ and its propagation direction along the unit vector $\hat{\mathbf{k}}$. Furthermore, we will use a '$\pm$' subscript to indicate the global direction of propagation: "+" when the wave travels from medium $1 \rightarrow 2$; and "−" when it travels from medium $2 \rightarrow 1$ (see Fig. 2.8). To complete the picture, we must specify the direction of oscillation (polarization) of either $\mathbf{E}$ or $\mathbf{B}$. We consider two explicit cases of polarization, one where $\mathbf{E}$ oscillates in the plane of incidence, $\mathbf{I}$, ($\mathbf{B}$ is then pointing out of the plane of incidence), denoted as the *p*-wave, or Transversal Electric (TE) wave; and the other where $\mathbf{E}$ oscillates out of the plane ($\mathbf{B}$ is then oscillating in the plane of incidence), which is denoted as the *s*-wave, or Transversal Magnetic (TM) wave. Any other polarization can be written as a linear combination of these two polarizations. Figure 2.8 represents the generalized situation of the problem where plane waves are incident from both sides of the interface onto it.

The projection of $\mathbf{k}$ on the interface is denoted as $\mathbf{q}$, and the wave-vector component perpendicular to it is denoted by $\pm\mathbf{w_i}$, where the sign follows the same sense of direction as stated above. Before we get to the boundary conditions for the problem, we must note that the periodicity along the interface must be conserved, thus q is equal for all the four wave vectors. In order to simplify the notations in all the discussion that follows, we will work, without loss of generality, in a unit system where the length unit is chosen in such a way that the vacuum wavelength of light is $2\,\pi$, and thus the length of the wave vector $|\mathbf{k}|$ in vacuum equal to one. Using elementary geometry, one has the following

$$\sin\theta_i = q/n_i \tag{2.52}$$

and

$$n_1{}^2 - w_1^2 = n_2{}^2 - w_2^2 \tag{2.53}$$

where θ_i are the angles of the wave vectors with respect to the normal of the interface. Equation (2.52) directly gives us *Snell's law of refraction* and *reflection* i.e.

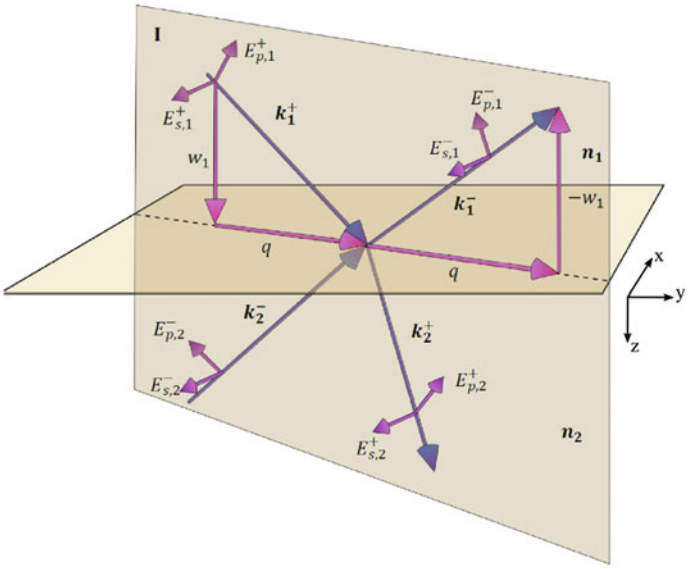

Fig. 2.8 A schematic representation of plane waves at a dielectric interface between two media with refractive indices n_i (for $i = 1, 2$). The waves are denoted by their wave vectors $\mathbf{k}_i^{\pm}$ depending upon their direction with respect to the interface; and the electric field polarizations as E_p or E_s depending on their orientations with respect to the plane of incidence **I** as shown. The vector $\mathbf{k}_i^{\pm}$ is resolved into two components $\pm\mathbf{w}_i$ and **q** perpendicular and in the interface

$n_1 \sin\theta_1 = n_2 \sin\theta_2$; and the wave vectors $\mathbf{k}_1^+$ and $\mathbf{k}_1^-$ have the same angle with the normal, θ_1.

Let us now establish the boundary conditions first by considering p-waves. In order to observe continuity in space, the tangential component of the electric field **E** and magnetic field **B** must be conserved across the interface. Thus we obtain

$$E^+_{p,1}\cos\theta_1 - E^-_{p,1}\cos\theta_1 = E^+_{p,2}\cos\theta_2 - E^-_{p,2}\cos\theta_2, \tag{2.54}$$

$$B^+_{p,1} + B^-_{p,1} = B^+_{p,2} + B^-_{p,2} \tag{2.55}$$

Using the relationship $|\mathbf{B}| = n_{\text{med}}\,|\mathbf{E}|$ and the fact that $\cos\theta_{1,2} = \frac{w_{1,2}}{n_{1,2}}$, we get

$$\frac{w_1}{n_1}E^+_{p,1} - \frac{w_1}{n_1}E^-_{p,1} = \frac{w_2}{n_2}E^+_{p,2} - \frac{w_2}{n_2}E^-_{p,2}, \tag{2.56}$$

$$n_1E^+_{p,1} + n_1E^-_{p,1} = n_2E^+_{p,2} + n_2E^-_{p,2} \tag{2.57}$$

These equations can be written in a compact matrix form as

$$\begin{pmatrix} \frac{w_1}{n_1} & -\frac{w_1}{n_1} \\ n_1 & n_1 \end{pmatrix} \begin{pmatrix} E^+_{p,1} \\ E^-_{p,1} \end{pmatrix} = \begin{pmatrix} \frac{w_2}{n_2} & -\frac{w_2}{n_2} \\ n_2 & n_2 \end{pmatrix} \begin{pmatrix} E^+_{p,2} \\ E^-_{p,2} \end{pmatrix} \tag{2.58}$$

Performing necessary matrix operations, Eq. (2.58) can be rewritten as

$$\begin{pmatrix} E^+_{p,1} \\ E^-_{p,1} \end{pmatrix} = \frac{1}{2} \begin{pmatrix} \frac{w}{n} + n & -\frac{w}{n} + n \\ -\frac{w}{n} + n & \frac{w}{n} + n \end{pmatrix} \begin{pmatrix} E^+_{p,2} \\ E^-_{p,2} \end{pmatrix} \tag{2.59}$$

where we use the notation $w = w_2/w_1$ and $n = n_2/n_1$. Let us denote the matrix in the Eq. (2.59) as $\hat{\mathbf{M}}_p$ for future reference. In the special case when an EM wave is incident from the side of the interface where the refractive index is n_1, we have

$$\begin{pmatrix} E^+_{p,1} \\ E^-_{p,1} \end{pmatrix} = \hat{\mathbf{M}}_p \begin{pmatrix} E^+_{p,2} \\ 0 \end{pmatrix} \tag{2.60}$$

Defining reflection and transmission coefficients as $R = E^-_1/E^+_1$ and $T = E^+_2/E^+_1$, we obtain

$$R_p = \frac{n^2 - w}{n^2 + w}, \tag{2.61}$$

and

$$T_p = \frac{2n}{n^2 + w} \tag{2.62}$$

For the case of s-waves, the boundary conditions can be written similar to equations (2.54) and (2.55) as

$$E^+_{s,1} + E^-_{s,1} = E^+_{s,2} + E^-_{s,2} \tag{2.63}$$

$$w_1 E^+_{s,1} - w_1 E^-_{s,1} = w_2 E^+_{s,2} - w_2 E^-_{s,2}, \tag{2.64}$$

Writing in the matrix form, we obtain,

$$\begin{pmatrix} E^+_{s,1} \\ E^-_{s,1} \end{pmatrix} = \frac{1}{2} \begin{pmatrix} 1 + w & 1 - w \\ 1 - w & 1 + w \end{pmatrix} \begin{pmatrix} E^+_{s,2} \\ E^-_{s,2} \end{pmatrix} \tag{2.65}$$

and the reflection and transmission coefficients are now given by

$$R_s = \frac{1 - w}{1 + w}, \tag{2.66}$$

and

$$T_s = \frac{2}{1+w} \tag{2.67}$$

Fig. 2.9 shows the reflection coefficients as a function of incident angle θ_1, or $\cos^{-1}(w_1/k_1)$. From Eq. (2.61) we find that R_p is zero when $w = n^2$ or $\cos\theta_1/n_1 = \cos\theta_2/n_2$, which can be seen in both cases of incidence as shown in the figure. The angle of incidence where the reflection coefficient vanishes is called *Brewster's angle*. Since from Snell's law we have $n_1/n_2 = \sin\theta_2/\sin\theta_1$, the situation only occurs when $\theta_1 + \theta_2 = \pi/2$ or $n_2/n_1 = \tan\theta_1$.

2.3.1 Total Internal Reflection

From Eq. (2.59), we get the amplitude of the $\mathbf{E}^+_{p,2}$

$$\mathbf{E}^+_{p,2} = \hat{\mathbf{e}}^+_{p,2}\frac{2E^+_{p,1}}{w/n+n} \tag{2.68}$$

where $\hat{\mathbf{e}}^+_{p,2} = \frac{w_2\hat{\mathbf{q}}-\mathrm{q}\hat{\mathbf{z}}}{n_2}$ is the unit vector along the polarization of the p-wave $\mathbf{E}^+_{p,2}$. Ignoring the time variation, the refracted plane wave can be written as $\propto \exp(-i\mathbf{k}^+_2\cdot\mathbf{r})$. Observing that $\mathbf{k}^+_2 = \mathrm{q}\hat{\mathbf{q}} + w_2\hat{\mathbf{z}}$, we can rewrite the exponential term as $\exp(i\mathbf{q}\cdot\boldsymbol{\rho}+iw_2z)$, where $\boldsymbol{\rho}$ is the two dimensional vector component of $\mathbf{r}$ within the interface. Using Eq. (2.53), w_2 can be written as

$$w_2 = \sqrt{n_2^2 - n_1^2 + w_1^2} \tag{2.69}$$

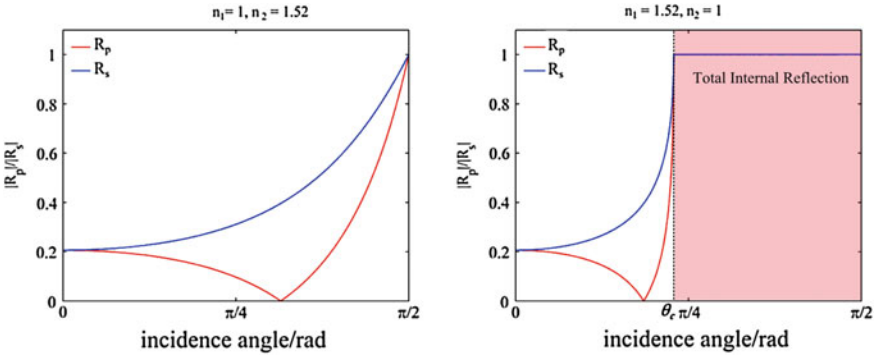

Fig. 2.9 Calculated reflection coefficients R_p and R_s as a function of the incident angle θ_1 for an air/glass interface for incidence from the air medium (*left*) and from the glass medium (*right*). The angle where the reflection coefficient for the p-waves is zero is the *Brewster's angle*. The critical angle θ_c, above which total internal reflection occurs is shown as well

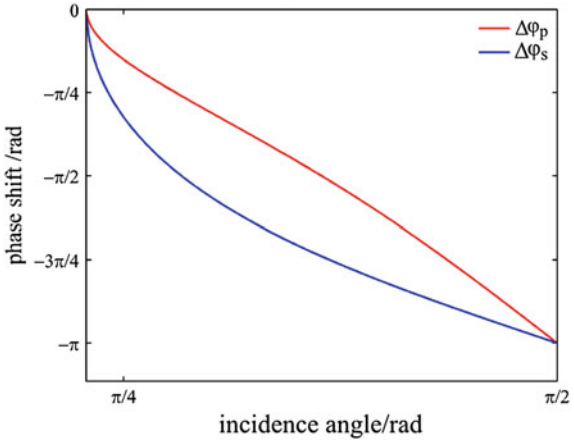

Fig. 2.10 The phase shift between the incident and the reflected p- and s-waves at the interface separating air and glass ($n = 1.52$). The plot shows for $\theta > \theta_c$, below which the phase shift is zero for both waves

This implies that w_2 becomes purely imaginary if $w_1 < \sqrt{n_1^2 - n_2^2}$. In this case, the spatial field dependence for the EM field represents a wave propagating along the interface in the plane of incidence (i.e. along the direction of $\hat{\mathbf{q}}$), but exponentially decaying perpendicular to the interface (along the z-axis). The amplitude decreases rapidly with the depth z, and the effective penetration depth is on the order of one wavelength. The wave is not transversal and is termed an evanescent wave. Remarkably, there is no transfer of energy across the interface and this phenomenon is called Total Internal Reflection (TIR). This can be shown by calculating the projection of the time averaged Poynting vector onto the normal of the interface, which is given by the expression

$$\frac{\mathrm{c}}{8\,\pi}\mathrm{Re}\left\{(\mathbf{E}\times\mathbf{B}^{*})\frac{w_2}{n_2}\right\} = \frac{\mathrm{c}}{8\pi}\mathrm{Re}\left\{n_2|\mathbf{E}|^2\frac{w_2}{n_2}\right\} = 0 \tag{2.70}$$

In the special situation when $w_1 = \sqrt{n_1^2 - n_2^2}$ or $\sin\theta_1 = n_2/n_1$ the wave propagates along the direction $\hat{\mathbf{q}}$, where total internal reflection starts, and the angle satisfying this condition is called "critical angle" (see Fig. 2.9).

It is important to note here that when TIR occurs, there is a phase shift between the incident and reflected waves. From the matrix equation (2.59) we get

$$\frac{E_{p,1}^{+}}{E_{p,2}^{+}} = \frac{1}{2}\left(\frac{w}{n} + n\right) \tag{2.71}$$

$$\frac{E^{-}_{p,1}}{E^{+}_{p,2}} = \frac{1}{2}\left(-\frac{w}{n} + n\right) \tag{2.72}$$

Since, w is imaginary, each factor contributes to an additional phase term $\exp(\pm \mathrm{i}\,\phi)$ and a total phase shift between the incident and reflected wave as

$$\Delta\phi_p = -2\tan^{-1}\left(\frac{\mathrm{Im}\, w}{n^2}\right) \tag{2.73}$$

Similar is the case for s-waves and one can calculate the phase shift as

$$\Delta\phi_s = -2\tan^{-1}\left(\mathrm{Im}\, w\right) \tag{2.74}$$

Figure 2.10 shows the calculated phase shifts for p-waves and s-waves at different incident angles. Since there is a phase shift between the incident and the total internally reflected rays, an interference is observed which leads to a shift in the reflected beam in the plane of the incidence towards the direction of propagation, which is known as *Goos-Hänchen Shift*.

2.3.2 Thin Layers and Frustrated Internal Reflection

We now consider the case where there are several thin layers stacked on top of each other. For the beginning, let us first consider the case where light traverses through two interfaces as shown in Fig. 2.11, separating three dielectric media ($n_i,\ i = 1, 2, 3$). To complete the picture, let us assign a thickness d for medium 2 sandwiched in between. Writing the transfer matrix for a p-wave at the second interface (between media 2 and 3), we have

$$\begin{pmatrix} E^{+b}_{p,2} \\ E^{-b}_{p,2} \end{pmatrix} = \frac{1}{2}\begin{pmatrix} \frac{w_{23}}{n_{23}} + n_{23} & -\frac{w_{23}}{n_{23}} + n_{23} \\ -\frac{w_{23}}{n_{23}} + n_{23} & \frac{w_{23}}{n_{23}} + n_{23} \end{pmatrix}\begin{pmatrix} E^{+}_{p,3} \\ E^{-}_{p,3} \end{pmatrix} \tag{2.75}$$

where $E^{\pm b}_{p,2}$ are electric fields at the second interface traveling in the medium 2 towards $(+)$ and away $(-)$ from the interface, $w_{ij} = w_i/w_j$ and $n_{ij} = n_i/n_j$. Similarly, at the first interface, another transfer matrix can be constructed

$$\begin{pmatrix} E^{+}_{p,1} \\ E^{-}_{p,1} \end{pmatrix} = \frac{1}{2}\begin{pmatrix} \frac{w_{12}}{n_{12}} + n_{12} & -\frac{w_{12}}{n_{12}} + n_{12} \\ -\frac{w_{12}}{n_{12}} + n_{12} & \frac{w_{12}}{n_{12}} + n_{12} \end{pmatrix}\begin{pmatrix} E^{+t}_{p,2} \\ E^{-t}_{p,2} \end{pmatrix} \tag{2.76}$$

where now $E^{\pm t}_{p,2}$ are electric fields at the first interface traveling in the medium 2 towards (+) and away (-) from the interface.

The connection between the two sets of fields inside the medium 2 is given by the phase difference when a wave travels a distance d in the medium.

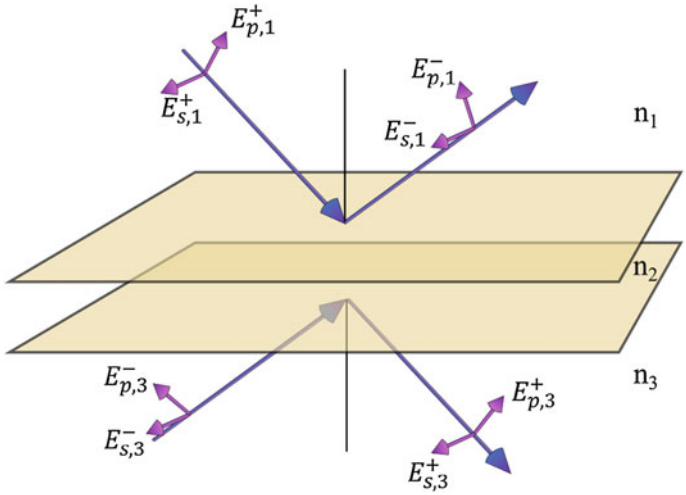

Fig. 2.11 A thin dielectric layer with refractive index n_2 is situated between two materials with refractive indices n_1 and n_3. The electric field vectors for the light rays above and below the first and second interface are shown here together with their polarizations

$$\begin{pmatrix} E^{+b}_{p,2} \\ E^{-b}_{p,2} \end{pmatrix} = \begin{pmatrix} e^{-iw_2 d} & 0 \\ 0 & e^{iw_2 d} \end{pmatrix} \begin{pmatrix} E^{+t}_{p,2} \\ E^{-t}_{p,2} \end{pmatrix} \tag{2.77}$$

where w_2 is the z-component of the wave-vector $\mathbf{k}_2$ in the medium. If w_2 is real then the matrix simply represents the phase accumulation for a plane wave propagating through the homogeneous medium of index n_2. Thus, the field in medium 3 can be written in terms of the field in medium 1 as

$$\begin{pmatrix} E^{+}_{p,1} \\ E^{-}_{p,1} \end{pmatrix} = \frac{1}{4} \begin{pmatrix} \frac{w_{12}}{n_{12}} + n_{12} & -\frac{w_{12}}{n_{12}} + n_{12} \\ -\frac{w_{12}}{n_{12}} + n_{12} & \frac{w_{12}}{n_{12}} + n_{12} \end{pmatrix} \begin{pmatrix} e^{-iw_2 d} & 0 \\ 0 & e^{iw_2 d} \end{pmatrix} \begin{pmatrix} \frac{w_{23}}{n_{23}} + n_{23} & -\frac{w_{23}}{n_{23}} + n_{23} \\ -\frac{w_{23}}{n_{23}} + n_{23} & \frac{w_{23}}{n_{23}} + n_{23} \end{pmatrix} \begin{pmatrix} E^{+}_{p,3} \\ E^{-}_{p,3} \end{pmatrix} \tag{2.78}$$

Before proceeding further, let us examine two important phenomena here. For the first case, let us assume that $n_3 = n_1 > n_2$. The transfer matrix $\hat{\mathbf{M}}_p$ for p-waves, considering boundary conditions for both the interfaces can be written as

$$\hat{\mathbf{M}}_p = \begin{pmatrix} \frac{w}{n} + n & -\frac{w}{n} + n \\ -\frac{w}{n} + n & \frac{w}{n} + n \end{pmatrix} \begin{pmatrix} \mathrm{e}^{-i\phi_2} & 0 \\ 0 & \mathrm{e}^{i\phi_2} \end{pmatrix} \begin{pmatrix} \frac{n}{w} + \frac{1}{n} & -\frac{n}{w} + \frac{1}{n} \\ -\frac{n}{w} + \frac{1}{n} & \frac{n}{w} + \frac{1}{n} \end{pmatrix} \tag{2.79}$$

where $w = w_2/w_1$ and $n = n_2/n_1$ and $\phi_2 = w_2 d$. Now, when there is TIR (i.e. w_2 is imaginary), the propagation matrix carries the loss of amplitude in the EM field when the plane wave propagates through the medium. $\hat{\mathbf{M}}_p$ can be simplified into the form of a 2×2 matrix as

$$\hat{\mathbf{M}}_p = \begin{pmatrix} A & B \\ B^* & A^* \end{pmatrix} \tag{2.80}$$

where $A = \cos\phi_2 - i/2\left(w/n^2 + n^2/w\right)\sin\phi_2$, $B = -i/2\left(w/n^2 - n^2/w\right)\sin\phi_2$. The matrix looks much similar for s-waves, $\hat{\mathbf{M}}_s$ can be obtained by putting $n = 1$ for the expressions of A and B. As we stated in the previous section, evanescent waves do not transmit any energy across the interface. However, if there is a third optically denser medium present, within one wavelength distance, from the first optically denser medium, these evanescent waves couple through and the energy is transmitted through the thin intermediate layer into the third medium. This phenomenon is similar to quantum tunneling and is called *frustrated internal reflection*, the term "Frustrated" appearing here due to the loss of energy in the reflected wave in the first optically rarer medium due to the effective evanescent-wave coupling. We will encounter this phenomenon later when discussing the interaction of en emitting electric dipole with a stack of layers.

In the case where $E_3^- = 0$, one has $E_1^+ = A \cdot E_3^+$. Therefore, the transmission coefficients are simply given by

$$T_{p,s} = \frac{E^+_{3,(p,s)}}{E^+_{1,(p,s)}} = \frac{1}{A_{p,s}} \tag{2.81}$$

Let us next consider the case where $n_1 = n_3 < n_2$. In this case, the component of the wave vector parallel to the interface $\mathbf{q}$ inside the thin layer can exceed the maximum possible $q = k_1$ in the media with the lower refractive index. Thus, if one considers a wave such that $k_2 \geq q > k_1$, one has total internal reflection at the interfaces. The evanescent waves outside cannot transfer energy away from the stack, and therefore one has multiple reflections inside the thin layer which acts as a *waveguide*. However, only for a few values of q, the sandwiched medium acts as a waveguide. These values depend on the thickness of the layer, the refractive indices of all the media involved and the polarization of the electric field inside the thin layer. These values can be found by realizing the conditions that $E_3^+ \neq 0$, $E_1^+ = 0$, which can be done by finding the solutions of $A = 0$. For p-waves, we have

$$A_p = \cos(w_2 d) - \frac{i}{2}\left(\frac{w}{n^2} + \frac{n^2}{w}\right)\sin(w_2 d) = 0 \tag{2.82}$$

where $w_2 = \sqrt{n_2^2 - q^2}$ and $k_2 \geq q > k_1$. The modes for the case of s-waves can be found similarly by solving for $A_s = 0$, where A_s is given by the expression

$$A_s = \cos(w_2 d) - \frac{i}{2}\left(w + \frac{1}{w}\right)\sin(w_2 d) \tag{2.83}$$

2.3.3 Fresnel's Equations for a Metal Surface

Let us now study the reflection and transmission properties of plane waves upon incidence on a metal surface. We follow the same notation as in all our previous sections (for example Sect. 2.3) and define n_1 as the dielectric medium above the interface and $\widetilde{n_2} = n_2 + i\kappa_2$ as the refractive index of the metal at a frequency ω. Let us first consider the case of p-waves. The electric field of a plane wave in medium 2 can be written as

$$\mathbf{E}^{\pm}_{p,2}(\mathbf{r}, t) = E^{\pm}_{p,2} e^{i(\mathbf{k}^{\pm}_2 \cdot \mathbf{r} - \omega t)} \hat{\mathbf{e}}^{\pm}_{2p} \tag{2.84}$$

The wave vector $\mathbf{k_2}^{\pm}$ can be written as $\mathbf{k}^{\pm}_2 = q\hat{\mathbf{q}} \pm w_2 \hat{\mathbf{z}}$ where $\mathbf{q}$ is the projection of the wave vector onto the interface whose magnitude is given by $q = n_1 \sin\theta_1 = \widetilde{n}_2 \sin\widetilde{\theta}_2$ and $w_2 = \sqrt{k_2^2 - q^2}$. Therefore, $\mathbf{k_2}^{\pm} \cdot \mathbf{r} = q(\hat{\mathbf{q}} \cdot \boldsymbol{\rho}) \pm w_2 z$, where $\boldsymbol{\rho}$ is a two dimensional vector within the interface. Using this relation, the electric field in the metal can be written as

$$\mathbf{E}^{\pm}_{p,2}(\mathbf{r}, t) = E^{\pm}_{p,2} e^{i[q(\hat{\mathbf{q}} \cdot \boldsymbol{\rho}) - \omega t]} e^{\pm i w_2 z} \hat{\mathbf{e}}^{\pm}_{2p} = E^{\pm}_{p,2} e^{i[q(\hat{\mathbf{q}} \cdot \boldsymbol{\rho}) \pm \mathrm{Re}(w_2) z - \omega t]} e^{\mp \mathrm{Im}(w_2) z} \hat{\mathbf{e}}^{\pm}_{2p} \tag{2.85}$$

Before proceeding further, we must understand the behavior of the electric fields represented by Eq. (2.85). The first part of the expression on the right represents a plane wave propagating in the direction of $\hat{\boldsymbol{\rho}}$ with a wave vector $\mathbf{q}$; whereas the second part represents a phase shift (real part of w_2) and an exponential modification of the magnitude (imaginary part of w_2) of the electric field $E^{\pm}_{p,2}$ with its propagation along z-direction. The magnitude entirely depends on the sign of the quantity $\mathrm{Im}\{w_2\}$ where,

$$w_2 = \sqrt{(n_2^2 - \kappa_2^2 - q^2) + 2in_2\kappa_2}. \tag{2.86}$$

The sign of the imaginary part of w_2 depends on the sign of the term $n_2\kappa_2$ (principal square root). From Eq. (2.51), we see that this product is directly proportional to the specific conductivity which cannot be a negative number. This leads to the fact that the magnitude of $\mathbf{E}^{+}_{p,2}$ declines with increasing z and for the case of $\mathbf{E}^{-}_{p,2}$, the magnitude falls exponentially with the decrease of z. In other words, the magnitude of an electromagnetic wave penetrating the metal surface ($z > 0$), falls of exponentially with depth. The magnitude falls down by a factor of e^{-1} for $z = 1/\mathrm{Im}\{w_2\}$. For normal incidence, $\mathrm{Im}\{w_2\} = \kappa_2\, \omega / c$ and hence, $\kappa(\omega)$ is also called the *extinction coefficient*. It represents the attenuation of the electromagnetic waves propagating through the medium.

While deriving Fresnel's equations for the reflection and transmission of plane waves for a metal surface, one must observe the same boundary conditions for the electric and magnetic fields at the interface as given in Sect. 2.3. The equations (2.54)

to (2.64) can be written similarly for the case of a complex refractive index, and the transformation matrix approach we built in that section is valid here. Hence, the reflection coefficient for the case of p- and s-waves respectively is given by

$$R_p = \frac{\widetilde{n}^2 - \widetilde{\mathrm{w}}}{\widetilde{n}^2 + \widetilde{\mathrm{w}}} \tag{2.87}$$

and,

$$R_s = \frac{1 - \widetilde{\mathrm{w}}}{1 + \widetilde{\mathrm{w}}} \tag{2.88}$$

where we used $\widetilde{\mathrm{w}} = \mathrm{w}_2/\mathrm{w}_1$ and $\widetilde{n} = n_2/n_1$. Figure 2.12 shows the reflectivity $(R \cdot R^*)$ and phase shift $\Delta\phi$ for p- and s-waves on a gold/air interface as a function of wavelength and incident angle θ_1. For normal incidence ($\theta_1 = 0$), $\Delta = \Delta\phi_p - \Delta\phi_s = -\pi$, whereas for grazing incidence, $\Delta = 0$. Between these two extreme cases, there exists an angle θ_i when $\Delta = -\pi/2$ and therefore a linearly polarized light is reflected as an elliptically polarized light. This angle is, in general, where the reflection coefficient for the p-waves is a non-zero minimum, and is called the *principle angle of incidence* [24].

2.4 The Oscillating Dipole

Any change of charge or current distribution in space produces an EM radiation. The most fundamental source of an EM wave is an oscillating electric dipole. Almost all fluorescent organic dyes can be well described as ideal electric dipole oscillators. In this section we extensively study the behavior of an oscillating electric dipole in a homogeneous environment which will be vital for our further theoretical discussion and the work in this thesis.

2.4.1 Dipole in a Homogeneous Environment

Let us consider a dipole at position $\mathbf{r} = 0$ oriented along the z-axis with a distance d between its two equal but opposite charges ($+q$ and $-q$) that are oscillating around the center with a frequency ω. We first derive the field $\mathbf{E(r)}$ when the time is frozen, i.e. the positions of the two charges are fixed in space. The potential ψ at a position $\mathbf{r}$ away from the dipole can be written as

$$\psi(r) = \frac{1}{\epsilon} q \left[\frac{1}{|\mathbf{r} - \mathbf{z}_+|} - \frac{1}{|\mathbf{r} - \mathbf{z}_-|} \right] = \frac{1}{\epsilon} q \left[\frac{|\mathbf{z}_- - \mathbf{z}_+| \cos\theta}{|\mathbf{r} - \mathbf{z}_+|\,|\mathbf{r} - \mathbf{z}_-|} \right] \tag{2.89}$$

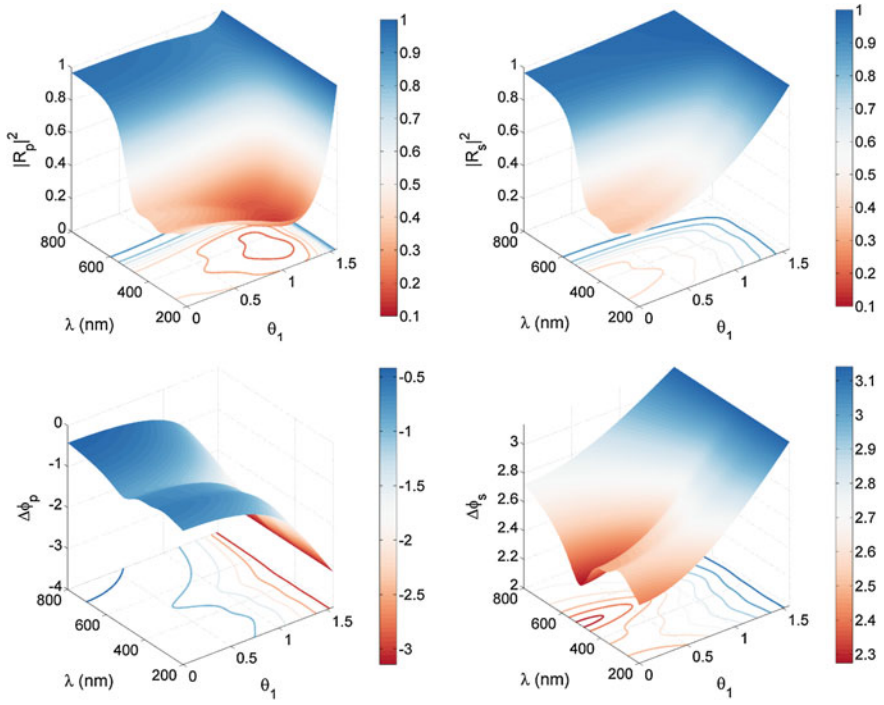

Fig. 2.12 Surface plots and contours showing the reflectivity and phase shifts for p- and s- waves on a gold/air interface. For each wavelength, the reflectivity $|R_p|^2$ reaches a non-zero minimum at a certain incidence angle θ_i as can be seen from the *top-left* surface plot. The *bottom* two plots show the phase shift for p- and s-waves

where $\mathbf{z}_{\pm}$ are the positions of the point charges, and θ is the angle between the line joining position $\mathbf{r}$ to the position of the dipole and the axis of the dipole. When the point of interest is far away from the dipole ($r >> d$), the product $|\mathbf{r} - \mathbf{z}_+|\,|\mathbf{r} - \mathbf{z}_-|$ can be simply approximated as r^2. Therefore, the Eq. (2.89) can be written as

$$\psi(r) = \frac{p\cos\theta}{\epsilon\, r^2} \tag{2.90}$$

$\mathbf{p}$ is the dipole moment defined as $\mathbf{p} = q\mathbf{d}$, where $\mathbf{d} = \mathbf{z}_- - \mathbf{z}_+$. The electric field $\mathbf{E}$ for the dipole can be calculated in the following way

$$\mathbf{E}(\mathbf{r}) = -\nabla\psi = -\left(\hat{\mathbf{r}}\frac{\partial}{\partial r} + \hat{\boldsymbol{\theta}}\frac{1}{r}\frac{\partial}{\partial\theta}\right)\psi = \frac{2p\cos\theta}{\epsilon\, r^3}\hat{\mathbf{r}} + \frac{p\sin\theta}{\epsilon\, r^3}\hat{\boldsymbol{\theta}} \tag{2.91}$$

Now $p\cos\theta$ can be written as $\hat{\mathbf{r}}\cdot\mathbf{p}$ and $p\sin\theta\hat{\boldsymbol{\theta}}$ as $\hat{\mathbf{r}}\times(\hat{\mathbf{r}}\times\mathbf{p})$. Substituting these identities in the Eq. (2.91) gives the relation

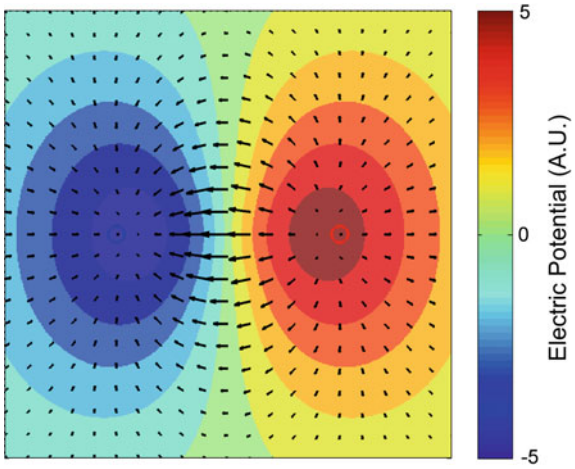

Fig. 2.13 Contour plot of electrostatic potential of a static dipole oriented horizontally showing electric field lines. The *red* and *blue circles* represent the positions of positive and negative charges respectively. The *arrows* show the direction and magnitude of electric field lines

$$\mathbf{E}(\mathbf{r}) = \frac{2\hat{\mathbf{r}}(\hat{\mathbf{r}} \cdot \mathbf{p})}{\epsilon r^3} + \frac{\hat{\mathbf{r}} \times (\hat{\mathbf{r}} \times \mathbf{p})}{\epsilon r^3} = \frac{3\hat{\mathbf{r}}(\hat{\mathbf{r}} \cdot \mathbf{p}) - \mathbf{p}}{\epsilon r^3} \tag{2.92}$$

This represents the field of a static electric dipole and it is a stationary electric field where no propagating EM radiation is generated. The static field is present close to the dipole whose strength decays rapidly as a r^{-3} distance relationship form the center of the dipole. The time-averaged Poynting vector is proportional to r^{-6}. No energy is transported away from the dipole in this case because anything that falls of faster than r^{-2} cannot carry energy away (Fig. 2.13).

EM waves are generated by non-stationary sources such as a non-uniformly moving point charge or an oscillating dipole. If we now want to calculate the EM radiation of an oscillating dipole, we need to take into account its temporal variation. Given non-zero $\rho(\mathbf{r}, t)$ and $\mathbf{j}(\mathbf{r}, t)$, which are now functions of time, it is not so straightforward to obtain unique solutions for the fields $\mathbf{E}(\mathbf{r}, t)$ and $\mathbf{B}(\mathbf{r}, t)$ from Maxwell's equations presented in Sect. 2.2. Information travels with a finite speed and is delayed in time and in order to incorporate time-varying dipole moments, one needs to involve retarded potentials with suitable gauge conditions. Here, we present an alternate way for obtaining the EM radiation which does not involve such a theoretical complexity.

Representing the time-variation of the oscillating dipole by the usual complex-valued notation $e^{-i\omega t}$ the positions of the two charges can be written as

$$z_{\pm} = \pm\frac{d}{2}e^{-i\,\omega\,t} \tag{2.93}$$

and their respective velocities by

$$v_{\pm} = \frac{dz_{\pm}}{dt} = \mp i \frac{d}{2} \omega e^{-i\omega t} \tag{2.94}$$

The current density, j is given by the sum of the product of charges with their respective velocities. Therefore,

$$j = -iqd\,\omega\, e^{-i\omega t} = -ip\,\omega\, e^{-i\omega t} \tag{2.95}$$

where $p = qd$ is the amplitude of the dipole moment. The dipole moment vector $\mathbf{p}$ is oriented along the direction from the negative to the positive charge. Therefore the vector $\mathbf{j}$ can be written as

$$\mathbf{j} = -i\,\omega\,\mathbf{p} e^{-i\omega t}\,\delta(\mathbf{r}) \tag{2.96}$$

where,

$$\delta(\mathbf{r}) = \int \frac{\mathrm{d}^3 k}{(2\pi)^3} e^{i\mathbf{k}\cdot\mathbf{r}} \tag{2.97}$$

is the Dirac delta function in three dimensions.

Let us now recall Maxwell's equations from Sect. 2.2 and apply to our oscillating dipole system. $\mathbf{E}(\mathbf{r}, t)$ can be written as $\mathbf{E}(\mathbf{r})e^{-i\omega t}$. Setting μ to unity (we consider non-magnetic materials in this thesis only), Eqs. (2.36) and (2.37), using Eq. (2.96) can be written as

$$\nabla \times \mathbf{B} = \frac{4\pi}{c}\mathbf{j} + \frac{1}{c}\frac{\partial \mathbf{E}}{\partial t} = -4\pi i k_0 \mathbf{p}\,\delta(\mathbf{r}) - ik_0\mathbf{E} \tag{2.98}$$

$$\nabla \times \mathbf{E} = -\frac{1}{c}\frac{\partial \mathbf{B}}{\partial t} = ik_0\mathbf{B} \tag{2.99}$$

where we set $k_0 = \omega/c$. Using equations (2.98) and (2.99) we get

$$\nabla \times \nabla \times \mathbf{E} = ik_0 \nabla \times \mathbf{B} = \epsilon k_0^2 \mathbf{E} + 4\pi k_0^2 \mathbf{p}\,\delta(\mathbf{r}) \tag{2.100}$$

Applying a spatial Fourier transform to the above equation, we get

$$-\mathbf{k} \times \mathbf{k} \times \widetilde{\mathbf{E}} - \epsilon k_0^2 \widetilde{\mathbf{E}} = (k^2 - \epsilon k_0^2)\widetilde{\mathbf{E}} - \mathbf{k}(\mathbf{k} \cdot \widetilde{\mathbf{E}}) = 4\pi k_0^2 \mathbf{p} \tag{2.101}$$

Multiplying both sides of Eq. (2.101) with $\mathbf{k}$, this simplifies to

$$\mathbf{k} \cdot \widetilde{\mathbf{E}} = -\frac{4\pi}{\epsilon}\mathbf{k} \cdot \mathbf{p} \tag{2.102}$$

Substituting Eq. (2.102) back in (2.101) we obtain

$$\widetilde{\mathbf{E}} = \frac{4\,\pi}{\epsilon(k^2 - \epsilon\, k_0^2)}\left[\epsilon\, k_0^2\mathbf{p} - \mathbf{k}(\mathbf{k}\cdot\mathbf{p})\right] \tag{2.103}$$

Passing back to real space from Fourier space, $\mathbf{E}(\mathbf{r})$ can be obtained using

$$\mathbf{E}(\mathbf{r}) = \int \frac{\mathrm{d}^3k}{(2\,\pi)^3}\widetilde{\mathbf{E}}(\mathbf{k})e^{i\mathbf{k}\cdot\mathbf{r}}$$

Using Eq. (2.103) we get

$$\mathbf{E}(\mathbf{r}) = \frac{4\,\pi}{\epsilon}\int \frac{\mathrm{d}^3k}{(2\,\pi)^3}\frac{\epsilon\, k_0^2\mathbf{p} - \mathbf{k}\,(\mathbf{k}\cdot\mathbf{p})}{\left(k^2 - \epsilon\, k_0^2\right)}e^{i\mathbf{k}\cdot\mathbf{r}} \tag{2.104}$$

Now, one can observe that

$$\boldsymbol{\nabla}\cdot\left(\mathbf{p}e^{i\mathbf{k}\cdot\mathbf{r}}\right) = i\,(\mathbf{k}\cdot\mathbf{p})e^{i\mathbf{k}\cdot\mathbf{r}}$$

and therefore,

$$\boldsymbol{\nabla}\left(\boldsymbol{\nabla}\cdot(\mathbf{p}e^{i\mathbf{k}\cdot\mathbf{r}})\right) = -\mathbf{k}(\mathbf{k}\cdot\mathbf{p})e^{i\mathbf{k}\cdot\mathbf{r}} \tag{2.105}$$

Using the last relationship, one can write the electric field $\mathbf{E}(\mathbf{r})$ as

$$\mathbf{E}(\mathbf{r}) = \frac{1}{2\,\pi^2\,\epsilon}\left(\epsilon\, k_0^2 + \boldsymbol{\nabla}\,(\boldsymbol{\nabla}\cdot)\right)\left[\mathbf{p}\int \frac{e^{i\mathbf{k}\cdot\mathbf{r}}}{k^2 - \epsilon\, k_0^2}\mathrm{d}^3k\right] \tag{2.106}$$

The integral on the right hand side can be simplified by switching into spherical coordinate system such that the vector $\mathbf{r}$ is along the polar axis and the dipole oriented at an angle α to this direction. Thus, $\mathbf{k}$ can be written as

$$\mathbf{k} = k\,(\sin\theta\cos\phi,\, \sin\theta\sin\phi,\, \cos\theta)$$

$$\therefore\ \mathbf{k}\cdot\mathbf{r} = kr\cos\theta$$

Using this, the integral can be treated as

$$\begin{aligned}\int \frac{e^{i\mathbf{k}\cdot\mathbf{r}}}{k^2 - \epsilon\, k_0^2}\mathrm{d}^3k &= \int_0^\infty \mathrm{d}k\, k^2 \int_0^\pi \mathrm{d}\theta\, \sin\theta \int_0^{2\,\pi} \mathrm{d}\phi\, \frac{e^{ikr\cos\theta}}{k^2 - \epsilon\, k_0^2} \\ &= 2\pi \int_0^\infty \mathrm{d}k\, k^2 \int_0^\pi \mathrm{d}\theta\, \sin\theta\, \frac{e^{ikr\cos\theta}}{k^2 - \epsilon\, k_0^2}\end{aligned}$$

by making the substitution $\zeta = \cos\theta$ in the second integral, we get

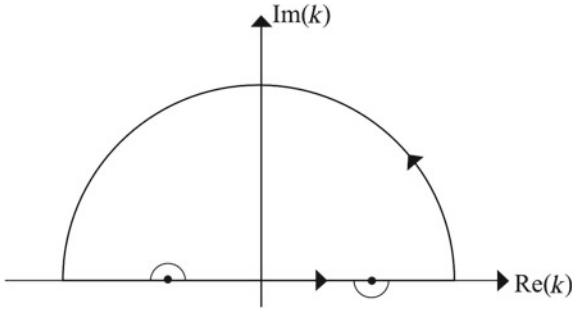

Fig. 2.14 Closed contour showing the inclusion of the pole at $+\sqrt{\epsilon}k_0$ for our integration

$$\int \frac{e^{i\mathbf{k}\cdot\mathbf{r}}}{k^2-\epsilon k_0^2}\mathrm{d}^3k = 2\pi\int_0^\infty \mathrm{d}k\, k^2 \frac{1}{ikr}\frac{e^{ikr}-e^{-ikr}}{k^2-\epsilon k_0^2}$$
$$= \frac{2\pi}{ir}\int_0^\infty \mathrm{d}k\, k\frac{e^{ikr}-e^{-ikr}}{k^2-\epsilon k_0^2}$$
$$= \frac{2\pi}{ir}\left[\int_0^\infty \mathrm{d}k\, k\frac{e^{ikr}}{k^2-\epsilon k_0^2} - \int_0^\infty \mathrm{d}k\, k\frac{e^{-ikr}}{k^2-\epsilon k_0^2}\right]$$

Substituting in the second integral $-k$ with k, we finally get

$$\int \frac{e^{i\mathbf{k}\cdot\mathbf{r}}}{k^2-\epsilon k_0^2}\mathrm{d}^3k = \frac{2\pi}{ir}\int_{-\infty}^\infty \mathrm{d}k\, k\frac{e^{ikr}}{k^2-\epsilon k_0^2} \tag{2.107}$$

The right hand side of Eq. (2.107) represents an integral over complex plane with two singularities $k = \pm\sqrt{\epsilon}k_0$. Using Cauchy's residue theorem,[3] we select a contour which includes only the outgoing waves from the dipole, which are physically reasonable. i.e. the pole at $k = +\sqrt{\epsilon}k_0$, as shown in Fig. 2.14. Since r is always positive, we take the positive imaginary values for k so that $e^{ikr} \to 0$ when $|\mathrm{Im}(k)| \to \infty$.

$$\frac{2\pi}{ir}\int_{-\infty}^\infty \mathrm{d}k\, k\frac{e^{ikr}}{k^2-\epsilon k_0^2} = \frac{2\pi}{ir}\oint_\Gamma \mathrm{d}k \quad k\frac{e^{i\sqrt{\epsilon}k_0 r}}{k^2-\epsilon k_0^2} \tag{2.108}$$

$$= 2\pi^2\frac{e^{ikr}}{r} \tag{2.109}$$

[3] If $f(z)$ has singularities at N points in space, then

$$\frac{1}{2\pi i}\oint_C f(z)\mathrm{d}z = \sum_{n=1}^{N}\mathrm{Res}(f, z_n)$$

Refer to "Complex Analysis" by Ahlfors [25].

Putting Eq. (2.109) in (2.106) we obtain the expression

$$\mathbf{E}(\mathbf{r}) = \frac{1}{\epsilon}\left(k^2 + \boldsymbol{\nabla}\left(\boldsymbol{\nabla}\cdot\right)\right)\left[\mathbf{p}\frac{e^{ikr}}{r}\right] \tag{2.110}$$

where we used $k = \sqrt{\epsilon}k_0$. When explicitly performing the differential operations on the r.h.s., one obtains

$$\begin{aligned}\boldsymbol{\nabla}\left(\boldsymbol{\nabla}\cdot\right)\left[\mathbf{p}\frac{e^{ikr}}{r}\right] &= \boldsymbol{\nabla}\left[\left(\frac{ik}{r} - \frac{1}{r^2}\right)(p\cos\alpha)\, e^{ikr}\right] \\ &= \left[\left(-\frac{k^2}{r} - \frac{2ik}{r^2} + \frac{2}{r^3}\right)(p\cos\alpha)\,\hat{\mathbf{r}} - \frac{1}{r}(p\sin\alpha)\,\hat{\boldsymbol{\theta}}\left(\frac{ik}{r} - \frac{1}{r^2}\right)\right] e^{ikr} \\ &= \left[\left(-\frac{k^2}{r} - \frac{2ik}{r^2} + \frac{2}{r^3}\right)(\mathbf{p}\cdot\hat{\mathbf{r}})\,\hat{\mathbf{r}} - \frac{1}{r}\hat{\mathbf{r}}\times\left(\hat{\mathbf{r}}\times\mathbf{p}\right)\left(\frac{ik}{r} - \frac{1}{r^2}\right)\right] e^{ikr}\end{aligned}$$

Finally, using the expansion $\hat{\mathbf{r}}\times\left(\hat{\mathbf{r}}\times\mathbf{p}\right) = \hat{\mathbf{r}}(\hat{\mathbf{r}}\cdot\mathbf{p}) - \mathbf{p}$ rearranging the terms, we find the electric field $\mathbf{E}(\mathbf{r}, t)$ of the dipole

$$\mathbf{E}(\mathbf{r}, t) = \left\{\frac{k^2}{r}\left[\mathbf{p} - \hat{\mathbf{r}}(\hat{\mathbf{r}}\cdot\mathbf{p})\right] + \left(\frac{ik}{r^2} - \frac{1}{r^3}\right)\left[\mathbf{p} - 3\hat{\mathbf{r}}(\hat{\mathbf{r}}\cdot\mathbf{p})\right]\right\} e^{ikr - i\,\omega t} \tag{2.111}$$

Equation (2.111) represents the complete electric field of an oscillating electric dipole. As one can see, if we set $k = 0$, it reduces to the electric field of a static dipole (2.92). This is where the velocity of light $c = 1/\sqrt{\epsilon}$ comes into the picture. If one takes $c = \infty$, $k = 0$ and the solution to the potential is an instantaneously varying static field governed by the dipole moment $\mathbf{p}$ at any time t.

The terms scaling with r^{-2} and r^{-3} constitute the near-field of the dipole which plays a major role when considering its interactions with another oscillating dipole in its vicinity or in an inhomogeneous environment such as close to a surface or inside a nanocavity. The part of the field scaling with r^{-1} is the far-field component which contributes to the transport of radiation energy away from the dipole.

The magnitude of the electric field depends on the length of the vector $\left[\mathbf{p} - \hat{\mathbf{r}}(\hat{\mathbf{r}}\cdot\mathbf{p})\right]$ which can be written as $p\sin\alpha$ where, α is the angle between $\mathbf{p}$ and the vector towards the point of interest $\mathbf{r}$ as shown in Fig. 2.15. It also scales as the inverse of the distance r. The direction of the field points towards the vector $\hat{\mathbf{r}}\times(\hat{\mathbf{p}}\times\hat{\mathbf{r}})$ which is perpendicular to $\mathbf{r}$ in the plane containing both the vectors $\mathbf{r}$ and $\mathbf{p}$. Thus, the amplitude of the electric field $\left|\mathbf{E}(\hat{\mathbf{p}})\right|$ along the direction of the dipole moment is zero at all times. Figure 2.16 shows the magnitude of the electric field in the plane of a dipole at a fixed time. The waves are propagating radially away from the center of the dipole with the electric field vector $\mathbf{E}(\mathbf{r})$ pointing in the direction perpendicular to the position vector $\mathbf{r}$ at each point.

The magnetic field can be derived by taking the curl of the electric field in Eq. (2.110) as follows

$$\mathbf{B}(\mathbf{r}) = \frac{c}{i\,\omega}\nabla \times \mathbf{E}(\mathbf{r}) = \frac{1}{ik_0}\nabla \times \left[\frac{1}{\epsilon}\left(k^2 + \nabla\,(\nabla\cdot)\right)\left[\mathbf{p}\frac{e^{ikr}}{r}\right]\right]$$

Since $\nabla \times (\nabla a)$, where a is a scalar field, is always zero, the above equation reduces to

$$\mathbf{B}(\mathbf{r}) = \frac{k^2}{ik_0\,\epsilon}\nabla \times \left[\mathbf{p}\frac{e^{ikr}}{r}\right]. \tag{2.112}$$

Assuming again that the dipole is along the $\hat{\mathbf{z}}$, this brings us to the expression

$$\mathbf{B}(\mathbf{r}, t) = \frac{\hat{\mathbf{r}} \times \mathbf{p}}{n_{\text{med}}}\left(\frac{k^2}{r} + \frac{ik}{r^2}\right)e^{ikr - i\,\omega\,t} \tag{2.113}$$

Note that here we used the relations $k = k_0\sqrt{\epsilon}$ and $\sqrt{\epsilon} = n_{\text{med}}$. The magnetic field lines can be drawn as concentric circles around the dipole vector $\mathbf{p}$ where the magnitude at point $\mathbf{r}$ is $\sim p \sin\alpha/r$ pointing normal to the plane containing $\mathbf{r}$ and $\mathbf{p}$. This result is also consistent to the fact that the field $\mathbf{B}$ is always perpendicular to the motion of charges or current direction. Thus the magnetic field does not perform any work on the oscillating dipole.

So far, we derived the complete radiation field of an oscillating dipole in a classical framework. Next we are interested in the angular distribution of the energy radiated away from the dipole, which we will consider in the following section.

2.4.1.1 Angular Radiation Distribution of an Oscillating Dipole

The magnitude of the Poynting vector $|\mathbf{S}|$ is proportional to $n_{\text{med}}\,|\mathbf{E}|^2$ and it points along the propagation direction $\hat{\mathbf{k}}$. Before we calculate the average power radiated

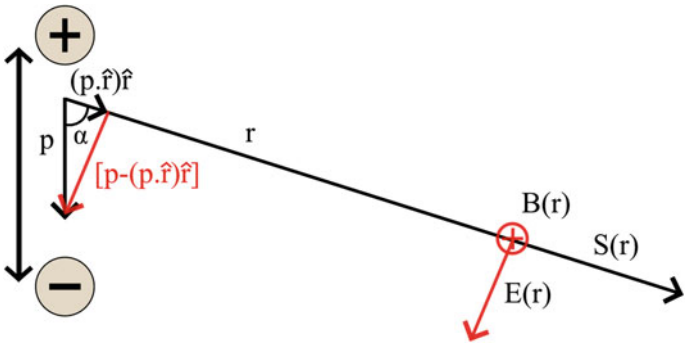

Fig. 2.15 A schematic showing the orientations of the dipole moment vector $\mathbf{p}$, and its projection along the line of sight $\mathbf{r}$. The vector shown in *red* represents the direction and the magnitude of the electric field vector $\mathbf{E}(\mathbf{r})$. The magnetic field $\mathbf{B}(\mathbf{r})$ points into the plane of the paper as shown. The Poynting vector $\mathbf{S}(\mathbf{r})$ always points in the direction of $\hat{\mathbf{r}}$

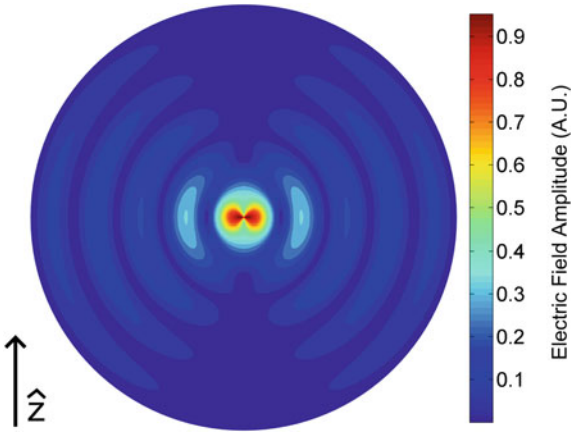

Fig. 2.16 Contour plot showing the magnitude of the far-field component of an oscillating dipole's electric field which is oriented along $\hat{\mathbf{z}}$. The radius of the image is $\approx 2.5\lambda$

by an oscillating dipole, it is important to mention that the fast decaying near-field components which scale with the distance as r^{-2} and r^{-3} do not contribute in the transport of energy away from the dipole, since the surface integrals of these components over a sphere of say radius r yield a net flux proportional to r^{-2} and r^{-4} respectively which vanish for large values of r ($r \ll \lambda$). Thus these near-field components are also termed the non-propagating components which can be neglected in the current section where we consider dipole oscillating in a homogeneous space. However, these near-field terms play a key role when studying dipole-dipole interactions and resonance energy transfer (such as FRET), or when considering dipoles situated close to an interface separating a dielectric or conducting medium. We shall study the latter situations closely in the forthcoming sections which will complete our theoretical foundation for Metal-Induced Energy Transfer (MIET). For now, we can approximate the electric and magnetic fields around an oscillating dipole as

$$\mathbf{E}(\mathbf{r}) \sim k^2 \left[\mathbf{p} - \hat{\mathbf{r}}(\hat{\mathbf{r}} \cdot \mathbf{p})\right] \frac{e^{ikr}}{r} \quad \text{and} \tag{2.114}$$

$$\mathbf{B}(\mathbf{r}) \sim k^2 \left[\hat{\mathbf{r}} \times \mathbf{p}\right] \frac{e^{ikr}}{r n_{\text{med}}} \tag{2.115}$$

Therefore the far-field Poynting vector is given by

$$\mathbf{S}(\mathbf{r}) \sim \frac{ck^4}{8\pi r^2 n_{\text{med}}} \hat{\mathbf{r}} \left[p^2 - (\hat{\mathbf{r}} \cdot \mathbf{p})^2\right] \tag{2.116}$$

$$= \frac{ck^4 p^2 \sin^2\theta}{8\pi r^2 n_{\text{med}}} \hat{\mathbf{r}} \tag{2.117}$$

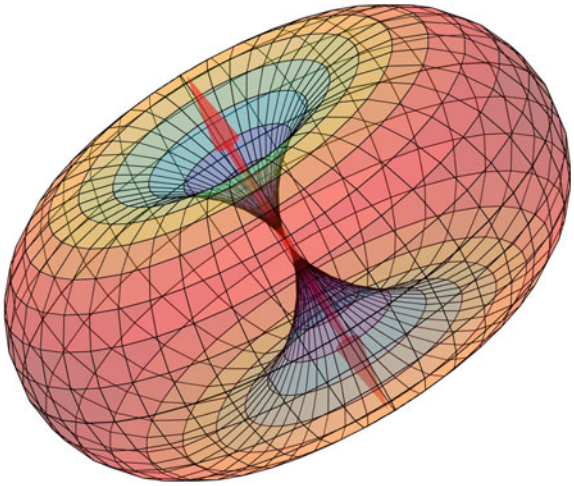

Fig. 2.17 The angular distribution of radiation from a dipole which is oscillating along the double *arrow* in the center. The distance of the surface from the center represents the probability of obtaining an emitted photon when the dipole is repeatedly excited. It follows the $\sin^2\alpha$ law, where α is the angle measured from the dipole moment vector **p**

Thus $\mathbf{S}(\mathbf{r})$ points away from the dipole's position and towards the point of interest. The magnitude of the flux density declines as the inverse of the square of the distance from the dipole. The total power radiated from an oscillating dipole is obtained by integrating the radial component of the Poynting vector over the sphere with radius r, and since the vector **S** is always normal to the surface, we have

$$S = \int_0^{\pi} \mathrm{d}\alpha \, \sin\alpha \int_0^{2\pi} \mathrm{d}\phi \, r^2 \frac{ck^4 p^2 \sin^2\alpha}{8\pi r^2 n_{\mathrm{med}}} = \frac{1}{3n_{\mathrm{med}}} ck^4 p^2. \tag{2.118}$$

Replacing k by $\sqrt{\epsilon}k_0$, we have

$$S = \frac{1}{3} cn_{\mathrm{med}} k_0^4 p^2. \tag{2.119}$$

The angular distribution of the power per solid angle $\mathrm{d}\Omega$ is given by

$$\frac{r^2 \mathrm{dS}}{\sin\alpha \mathrm{d}\alpha \mathrm{d}\phi} = \frac{cn_{\mathrm{med}} k_0^4 p^2}{8\,\pi} \sin^2\alpha \tag{2.120}$$

which directly gives the $\sin^2\alpha$ dependence of the radiation power from the dipole, where α is measured from the dipole's axis. Thus, the angular distribution looks like a torus with its axis along the dipole moment vector **p**. This is shown in Fig. 2.17.

The total power radiated by the dipole can also be calculated using the integral over the normal component of the time-averaged Poynting vector through a surface

enclosing the source

$$S = \oiint (\langle \mathbf{S} \rangle \cdot \hat{\mathbf{n}}) \mathrm{d}A \tag{2.121}$$

Using the Divergence theorem,[4] this can be written as

$$\begin{aligned} S &= \int_V \langle \nabla \cdot \mathbf{S} \rangle \, \mathrm{d}V = \frac{c}{4\pi} \int_V \langle \nabla \cdot (\mathbf{E} \times \mathbf{B}) \rangle \, \mathrm{d}V \\ &= \frac{c}{4\pi} \int_V \langle [(\nabla \times \mathbf{E}) \cdot \mathbf{B} - \mathbf{E} \cdot (\nabla \times \mathbf{B})] \rangle \, \mathrm{d}V \end{aligned}$$

Plugging in Maxwell's equations and taking the time average, this yields

$$S = -\frac{1}{2} \mathrm{Re} \left(\int_V \mathbf{E} \cdot \mathbf{j}^* \mathrm{d}V \right) \tag{2.122}$$

where $\mathbf{j}$ is the current density in the source. Thus, the radiation power is equal to the negative work done per unit of time by the field acting on the source. Using the current density for the oscillating dipole given by the Eq. (2.96), the total power can be written as

$$S = \frac{1}{2} \omega \, \mathbf{p} \cdot \mathrm{Im} \, (\mathbf{E}) \tag{2.123}$$

From a physics point of view, the above equation translates into the fact that the power radiated by an electric dipole is proportional to that component of the electric field which is along the direction of the dipole's axis and which is by $\pi/2$ out of phase with respect to the oscillation of the dipole moment.

The most important point to note from the Eq. (2.119) is the $k^4 \sim \lambda^{-4}$ dependence of the radiation power. The same law holds true for Rayleigh scattering theory of light, such as on density variations, which are smaller in size than the wavelength of the EM radiation scattered by them. Rayleigh scattering results from the electric polarization of the gas molecules due to their interaction with the radiation causing them to behave as oscillating dipoles. Thus, the above theory can be also applied to calculate the field around scattering particles. As shown in the above relation, the scattering cross section increases inversely proportional to the fourth power of the wavelength, and therefore the sky appears blue in color. Another interesting observation is the direct dependence of the radiation power on the refractive index of the medium. A dipole radiates more energy per unit of time if it is situated inside a medium of higher refractive index such as glass ($n = 1.5$) or water ($n = 1.33$). In a quantum mechanical picture, this translates to the fact that the excited molecules

[4] If $\mathbf{F}$ is a continuously differentiable vector over a volume V and its neighborhood, then $\int_v (\nabla \cdot \mathbf{F}) \mathrm{d}V = \oiint_A (\mathbf{F} \cdot \mathrm{d}\mathbf{A})$, where the vector element $\mathrm{d}\mathbf{A}$ points normal at each point to the surface of the volume V. For derivation, refer to [26].

return faster from their excited state to the ground state when placed in such media. In other words, the average lifetime of the excited state τ_f is shorter in water or glass as compared to air. The purely radiative decay rate, or spontaneous emission rate of a classical dipole oscillator is given by the ratio of the average radiation power of the dipole and its total initial energy. Assuming no damping in the oscillations, which will be considered in a later section, the spring constant is given by $k = \omega^2 m$, where m is the effective mass of the dipole and ω is the angular frequency of the oscillating spring system. If x_0 is the initial oscillation amplitude, the initial energy of the oscillation system is given by

$$U_0 = \frac{1}{2} k x_0^2 = \frac{1}{2} m \overset{2}{\omega} \frac{p_0^2}{q^2}. \tag{2.124}$$

The radiation power is the rate of change of this initial energy which is given by Eq. (2.119).

$$\therefore \frac{\mathrm{d}U}{U_0} = -\frac{2}{3} \frac{q^2 \omega^2 n_{\mathrm{med}}}{mc^3} \mathrm{d}t \tag{2.125}$$

which gives us the radiative rate κ_0 of the dipole.

$$\kappa_0 = \frac{2}{3} \frac{q^2 \omega^2 n_{\mathrm{med}}}{mc^3} \tag{2.126}$$

which is the inverse excited state lifetime (if there are no other de-excitation channels).

In the next section, we will study the behavior of a dipole emitter situated close to an interface separating two such dielectric media.

2.4.2 *Dipole on a Planar Dielectric Interface*

So far, we studied the properties of a dipole oscillating in a homogeneous environment. For our discussion in this section, let us consider a dipole situated on top of an interface separating the upper media ($z < 0$) with dielectric constant ϵ_1 and a lower medium ($z > 0$) with dielectric constant ϵ_2. Let the dipole moment vector be $\mathbf{p}$ at position $\mathbf{r}_0$. Let us further consider that $\mathbf{r_0}$ is a point in the medium 1, $z_0 < 0$. First, we write down the plane wave representation of the dipole's field in a homogeneous space with a dielectric constant ϵ_1 using (2.104).

$$\mathbf{E}(\mathbf{r}) = \frac{4\pi}{\epsilon_1} \int \frac{\mathrm{d}^3 k}{(2\pi)^3} \frac{\epsilon_1 k_0^2 \mathbf{p} - \mathbf{k}\,(\mathbf{k} \cdot \mathbf{p})}{\left(k^2 - \epsilon_1 k_0^2\right)} e^{i\mathbf{k}\cdot\mathbf{R}} \tag{2.127}$$

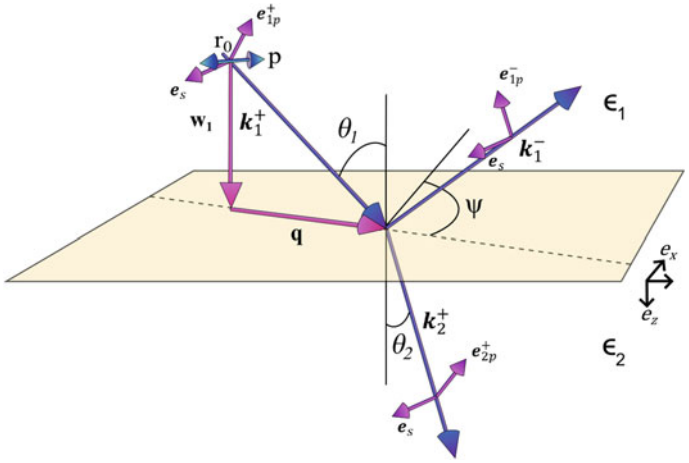

Fig. 2.18 The general geometry of the vectors considered in this section. The interface separates two media ϵ_1 and ϵ_2 as shown. The unit vectors $\hat{\mathbf{e}}^{\pm}_{ip}$ represent the directions of electric field vectors in the plane of incidence, whereas the unit vectors $\hat{\mathbf{e}}_s$ point in the direction perpendicular to the plane of incidence. θ_1 and θ_2 are the angles of the vectors $\mathbf{k}_1^+$ and $\mathbf{k}_2^+$ with respect to the normal of the interface, and ψ is the angle the plane of incidence makes with respect to a fixed x-axis. $\mathbf{r}_0$ marks the position of the dipole $\mathbf{p}$. Note that $\mathbf{p}$ is doubly degenerate, and hence we show using a double arrow

where $\mathbf{R} = \mathbf{r} - \mathbf{r_0}$. Let us denote, as before, by $\mathbf{q}$ and w the horizontal (parallel to the interface) and vertical (orthogonal to interface) components of the wave vector $\mathbf{k}$. Performing in the above plane wave representation the integration over w and applying Cauchy's residue theorem leads to the so-called Weyl representation of the electric field of an oscillating dipole in homogeneous space,

$$\mathbf{E}(\mathbf{r}) = \frac{i}{2\,\pi\,\epsilon_1}\int \mathrm{d}^2\mathbf{q}\,\frac{\left[k_1^2\mathbf{p} - \mathbf{k}_1^{\pm}(\mathbf{k}_1^{\pm}\cdot\mathbf{p})\right]}{w_1}\,e^{i\left[\mathbf{q}\cdot(\boldsymbol{\rho}-\boldsymbol{\rho}_\mathbf{0}) - w_1|z-z_0|\right]} \tag{2.128}$$

where $\mathbf{k}_j^{\pm} = \{\mathbf{q}, \pm w_j\}$ and $w_1(q) = \sqrt{k_1^2 - q^2}$ with $\mathbf{k_1} = \sqrt{\epsilon_1}\mathbf{k_0}$, and $\mathbf{k_1}^+$ applies for $z > z_0$ and $\mathbf{k_1}^-$ applies for $z < z_0$. When applying Cauchy's residue theorem, we have taken into account only the pole $w_1 = +\sqrt{k_1^2 - q^2}$ with positive real or positive imaginary value so that the Weyl representation integrates only over outgoing (or with distance exponentially decaying) plane waves, but not incoming or exponentially increasing plane waves (Fig. 2.18).

The vector $k_1^2\mathbf{p} - \mathbf{k}_1^{\pm}(\mathbf{k}_1^{\pm}\cdot\mathbf{p})$ is a projection of $\mathbf{p}$ perpendicular to the direction of $\mathbf{k}_1^{\pm}$, and can thus be expanded into a system of two orthogonal unit vectors which are both orthogonal to $\mathbf{k}_1^{\pm}$, in particular

$$\hat{\mathbf{e}}_{1p}^{\pm} = \frac{1}{k_1}\left(\frac{\pm w_1 q_x}{q}, \frac{\pm w_1 q_y}{q}, -q\right)$$

and

$$\hat{\mathbf{e}}_s = \frac{1}{q}(-q_y, q_x, 0)$$

Both these vectors are indeed perpendicular to $\mathbf{k}_1^{\pm} = \{q_x, q_y, \pm w_1\}$, whereas $\hat{\mathbf{e}}_{1p}^{\pm}$ lies within the plane which is spanned by $\mathbf{k}_1^{\pm}$ and the normal to the interface (p-wave), and $\hat{\mathbf{e}}_s$ lies parallel to the interface (s-wave). Thus, the Weyl representation can be rewritten as

$$\mathbf{E}(\mathbf{r}) = \frac{ik_0^2}{2\pi}\iint \frac{\mathrm{d}\mathbf{q}}{w_1}\left[\hat{\mathbf{e}}_{1p}^{\pm}(\hat{\mathbf{e}}_{1p}^{\pm}\cdot\mathbf{p}) + \hat{\mathbf{e}}_s(\hat{\mathbf{e}}_s\cdot\mathbf{p})\right] e^{i\left[\mathbf{q}\cdot(\boldsymbol{\rho}-\boldsymbol{\rho}_0)+w_1|z-z_0|\right]} \tag{2.129}$$

Now it is obvious that the Weyl representation (2.129) is an expansion of the dipole's electric field over plane p- and s-waves. If w_1 is imaginary, they are which decay exponentially with distance away from the plane of the dipole ($z = z_0$). In order to calculate the complete field, one now needs to calculate the fields reflected by and transmitted through the interface, which can be done in a straightforward way by using Fresnel's relations that we had derived in Sect. 2.3. These fields are given by

$$\mathbf{E}_R(\mathbf{r}) = \frac{ik_0^2}{2\pi}\iint \frac{\mathrm{d}\mathbf{q}}{w_1}\left[\hat{\mathbf{e}}_{1p}^{-}R_p(\hat{\mathbf{e}}_{1p}^{+}\cdot\mathbf{p}) + \hat{\mathbf{e}}_s R_s(\hat{\mathbf{e}}_s\cdot\mathbf{p})\right] e^{i\left[\mathbf{q}\cdot(\boldsymbol{\rho}-\boldsymbol{\rho}_0)+w_1|z_0|-w_1 z\right]}, \tag{2.130}$$

and

$$\mathbf{E}_T(\mathbf{r}) = \frac{ik_0^2}{2\pi}\iint \frac{\mathrm{d}\mathbf{q}}{w_1}\left[\hat{\mathbf{e}}_{2p}^{+}T_p(\hat{\mathbf{e}}_{1p}^{+}\cdot\mathbf{p}) + \hat{\mathbf{e}}_s T_s(\hat{\mathbf{e}}_s\cdot\mathbf{p})\right] e^{i\left[\mathbf{q}\cdot(\boldsymbol{\rho}-\boldsymbol{\rho}_0)+w_1|z_0|+w_2 z\right]}. \tag{2.131}$$

where we have introduced also the unit vector

$$\hat{\mathbf{e}}_{2p}^{+} = \frac{1}{k_2}\left(\frac{w_2 q_x}{q}, \frac{w_2 q_y}{q}, -q\right)$$

which is perpendicular to $\mathbf{k}_2^{+} = \{q_x, q_y, w_2\}$ with $w_2(q) = \sqrt{k_2^2 - q^2}$, and $R_{p,s}$ and $T_{p,s}$ are Fresnel's q-dependent reflection and transmission coefficients for plane p- and s-waves, respectively. Here, Eq. (2.130) is the reflected field ($z < 0$), and (2.131) is the transmitted field ($z > 0$). The term $e^{iw_1|z_0|}$ in both the reflected and transmitted fields takes into account the additional phase shift due to the plane wave propagation

form the dipole's position to the interface. Two important points can be read off from Eq. 2.131

1. The magnitude of the transmitted and reflected electric field depends on the orientation of the dipole vector $\mathbf{p}$ with respect to the plane of incidence. This is taken care of by the scalar products $\hat{\mathbf{e}}_{jp}^{\pm} \cdot \mathbf{p}$ and $\hat{\mathbf{e}}_s \cdot \mathbf{p}$.
2. The magnitudes of these electric fields clearly depend on the reflection and transmission coefficients $T_{p,s}$ and $R_{p,s}$, which are themselves functions of the angle of incidence and thus q of the plane waves with respect to the interface.

Let us now examine two important particular cases. In the first case, when $n_1 < n_2$ i.e., the dipole is in an optically rarer medium, such as water, on top of an optically denser medium, such as glass. In this case, all propagating waves in medium 1 are also propagating in medium 2 (since $w_2 = \sqrt{k_2^2 - k_1^2 + w_1^2}$ which is always real for $w_1 \leqslant k_1$ and $k_2 > k_1$). However, the amplitude of vector $\mathbf{q}$ can be larger than k_1 (it actually can go up to infinity). Thus, for the range of q-values with $k_1 < q \leq k_2$, one has non-propagating and exponentially decaying plane waves in medium 1 ($i w_1 |z_0|$ is real and negative), which, however, become propagating in medium 2, contributing to the far field radiation in the lower half-space. This is similar to frustrated internal reflection which we studied before. We had seen that this process results in an energy reduction of the reflected plane (as compared to TIR) and a partial energy transfer to the denser medium beneath the thin layer. In the situation here, one can visualize this as a dipole losing more energy per time than one within a homogeneous medium 1 without any interface (energy tunneling into denser medium). This leads to an increase in total radiated power S and, as a resulting, to an decrease of the excited state lifetime τ_f. Finally, for values of q larger than k_2, all plane waves are exponentially decaying, and they do not contribute to any far-field energy propagation. The second case is the opposite, when the dipole is located in the optically denser medium ($n_1 > n_2$). In this case, there exist propagating plane waves in medium 1 which cannot propagate in medium 2 (for $k_2 < q \leq k_1$). For these values of q, the absolute values of the reflection coefficients R_p and R_s are equal to one, and depending upon the distance of the emitter from the surface, constructive or destructive interference with the directly emitted plane wave along $\mathbf{k}_1^-$ takes place in medium 1. In medium 2, these plane waves are evanescent and exponentially decay with distance z.

2.4.2.1 Angular Distribution of Radiation of a Dipole Near a Dielectric Interface

In the upper half-space (medium 1), the angular distribution of radiation can be calculated from the time-averaged Poynting vector ($\mathbf{S}(\mathbf{r}) \propto |\mathbf{E}|^2$) using the dipole's direct field together with the reflected field along direction $\mathbf{k}_1^-$. Using the electric fields from Eqs. (2.129) and (2.130), we find that the energy flux radiated into a solid angle element $d\Omega^2 = (q/w_1 k_1) \mathrm{d}q \mathrm{d}\psi$ into the upper half-space ($z < 0$) along direction ($\mathbf{q}$, w_1) is proportional to

$$\frac{\mathrm{d}^2 S_u}{\mathrm{d}\Omega^2} \propto \frac{k_0^4 p^2}{4\pi^2} \left| \left[\hat{\mathbf{e}}_{1p}^{-} (\hat{\mathbf{e}}_{1p}^{-} \cdot \mathbf{p}) + \hat{\mathbf{e}}_s (\hat{\mathbf{e}}_s \cdot \mathbf{p}) \right] + \left[\hat{\mathbf{e}}_{1p}^{-} R_p (\hat{\mathbf{e}}_{1p}^{+} \cdot \mathbf{p}) + \hat{\mathbf{e}}_s R_s (\hat{\mathbf{e}}_s \cdot \mathbf{p}) \right] e^{2iw_1|z_0|} \right|^2 \tag{2.132}$$

The exponential term at the end of the reflected term represents the additional phase shift due to the path difference between the plane directly emitted by the dipole towards $\mathbf{k}_1^-$, and the plane wave which first propagates towards the interface along $\mathbf{k}_1^+$, and which is then reflected by it towards $\mathbf{k}_1^-$. Since p and s-waves are orthogonal to each other, the modulus can be split into two terms each containing one of these components separately

$$\frac{\mathrm{d}^2 S_u}{\mathrm{d}\Omega^2} \propto \frac{k_0^4 p^2}{4\pi^2} \left[\left| \left[\hat{\mathbf{e}}_{1p}^{-} + R_p \hat{\mathbf{e}}_{1p}^{+} e^{2iw_1|z_0|} \right] \cdot \mathbf{p} \right|^2 + \left| \left[1 + R_s e^{2iw_1|z_0|} \right] (\hat{\mathbf{e}}_s \cdot \mathbf{p}) \right|^2 \right] \tag{2.133}$$

Similarly, the energy flux density radiated into a solid angle element $d\Omega^2 = (q/w_2 k_2)\mathrm{d}q\mathrm{d}\psi$ into the lower half-space ($z > 0$) along direction ($\mathbf{q}$, w_2) is given by

$$\frac{\mathrm{d}^2 S_l}{\mathrm{d}\Omega^2} \propto \frac{k_0^4 p^2}{4\pi^2} \left| \frac{w_2}{w_1} \right|^2 \left[\left| T_p \hat{\mathbf{e}}_{1p}^{+} \cdot \mathbf{p} \right|^2 + \left| T_s \hat{\mathbf{e}}_s \cdot \mathbf{p} \right|^2 \right] e^{-2\mathrm{Im}(w_1)|z_0|} \tag{2.134}$$

The proportionality factors for each case can be obtained by considering the limiting case when the refractive indices of both media are identical, thus setting $R_p = R_s \equiv 0$ and $T_p = T_s \equiv 1$. By comparing the result with the angular distribution of radiation for a dipole in a homogenous medium with refractive index $n = n_1 = n_2$, i.e. with $(cnk_0^4/8\,\pi)\left[p^2 - (\hat{\mathbf{r}} \cdot \mathbf{p})^2\right]$, one finds the proportionality factors as $\pi\, cn/2$. This leads to the final expressions

$$\frac{\mathrm{d}^2 S_u}{\mathrm{d}\Omega^2} = \frac{cn_1 k_0^4 p^2}{8\,\pi} \left[\left| \left[\hat{\mathbf{e}}_{1p}^{-} + R_p \hat{\mathbf{e}}_{1p}^{+} e^{2iw_1|z_0|} \right] \cdot \mathbf{p} \right|^2 + \left| \left[1 + R_s e^{2iw_1|z_0|} \right] (\hat{\mathbf{e}}_s \cdot \mathbf{p}) \right|^2 \right] \tag{2.135}$$

and

$$\frac{\mathrm{d}^2 S_l}{\mathrm{d}\Omega^2} = \frac{cn_2 k_0^4 p^2}{8\,\pi} \left| \frac{w_2}{w_1} \right|^2 \left[\left| T_p \hat{\mathbf{e}}_{1p}^{+} \cdot \mathbf{p} \right|^2 + \left| T_s \hat{\mathbf{e}}_s \cdot \mathbf{p} \right|^2 \right] e^{-2\mathrm{Im}(w_1)|z_0|} \tag{2.136}$$

Figure 2.19 shows the dramatic change of the angular distribution of radiation for an emitting dipole on an air/glass interface as compared to the toroidal distribution in a homogeneous medium. Note that the emission of a vertical dipole is symmetric around the vertical axis, but not for a horizontal dipole. The enhanced radiation into the glass medium is one of the key reasons why inverted microscopes that look from the glass side should be preferred for single-molecule detection and sensitive bioimaging. The angular radiation distribution of a dipole on the interface for various

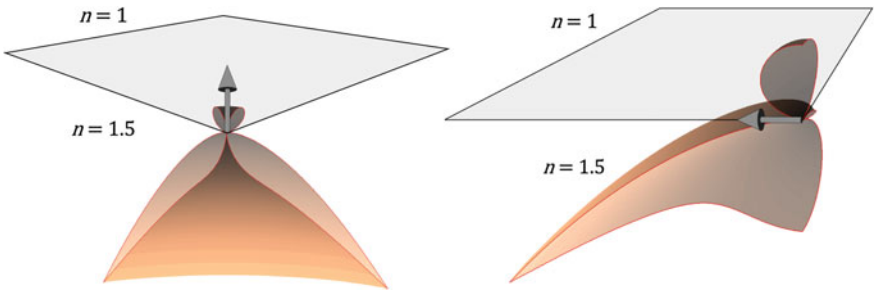

Fig. 2.19 Angular distribution of radiation of a vertical (*left*) and a parallel (*right*) dipole on top of an air/glass interface

values of the refractive index of the lower half space is shown in Fig. 2.20. For comparison, we also show the emission when there is no interface, i.e. $n_1 = n_2$. A can be seen, the energy emitted into the optically denser medium is much higher for a vertical dipole than for a horizontal dipole. Moreover, most of the energy is emitted at high emission angles, which requires a high Numerical Aperture (N.A.) objective to collect this emission efficiently. The reason is that plane wave components which are evanescent in the dipole's medium can tunnel into the optically denser medium of the lower half space where they become propagating, carrying away energy. Figure 2.21 below shows the distribution for various values of dipole orientation angles towards the interface.

2.4.2.2 Radiation Power of a Dipole on Top of a Dielectric Interface

The total power radiated by the dipole is given by the integral of angular distribution of radiation over all directions.

$$S = \int_0^{\pi/2} \mathrm{d}\theta_1 \sin\theta_1 \int_0^{2\pi} \mathrm{d}\psi \frac{\mathrm{d}^2 S_u}{\mathrm{d}\Omega^2} + \int_0^{\pi/2} \mathrm{d}\theta_2 \sin\theta_2 \int_0^{2\pi} \mathrm{d}\psi \frac{\mathrm{d}^2 S_l}{\mathrm{d}\Omega^2} \tag{2.137}$$

where θ_1 and θ_2 are the angles of wave vectors in media 1 and 2 ($\mathbf{k_1^-}$ and $\mathbf{k_2^+}$), respectively, and which are connected to the value of q via $\sin\theta_i = q/k_i$, for $i = 1, 2$. Thus, Eq. 2.137 takes the form

$$S = \int_0^{k_1} \mathrm{d}q \frac{q}{k_1 w_1} \int_0^{2\pi} \mathrm{d}\psi \frac{\mathrm{d}^2 S_u}{\mathrm{d}\Omega^2} + \int_0^{k_2} \mathrm{d}q \frac{q}{k_2 w_2} \int_0^{2\pi} \mathrm{d}\psi \frac{\mathrm{d}^2 S_l}{\mathrm{d}\Omega^2} \tag{2.138}$$

The upper limits for the integrations over q in the equation above are k_1 and k_2 for the upper and lower half-space, respectively. They represent the maximum possible projections of the wave vecotr into the plane of the interface for propagating waves in the respective half-space. The total power of emission S obtained is inversely proportional to the excited state lifetime of the dipole. In other words, the ratio of S with the total power of emission of a free dipole in a homogeneous medium of

refractive index n_1 (S_0), where S_0 is the total power of a dipole in vacuum ($n_1 = 1$), gives us the inverse of the ratio of the excited state lifetimes in both cases.

It can be shown that the total emission power of a dipole with arbitrary orientation α towards the vertical axis is given by the sum of the emission of a parallel and a vertical dipole with dipole moments which are its projections on the horizontal and vertical axis, respectively

$$S(\alpha, z_0) = S_{tot\,\perp}(z_0)\cos^2\alpha + S_{tot\,\parallel}(z_0)\sin^2\alpha \tag{2.139}$$

When the dipole is situated in the optically rarer medium close to the interface, $|z_0| < \lambda$, non-propagating near-field modes of the dipole can tunnel into the optically denser medium where they become propagating, which leads to an increase of the total radiation power. This can be observed as a faster decay of the excited state of a fluorescing molecule. An inverse effect takes place when the molecule is situated in the optically denser medium. Figure 2.22 shows the total power radiated by a dipole at different positions above a glass/water interface for both, horizontal and vertical orientations. Let us notice that the radiation power shows a periodic behavior with distance from the interface, with a period of $\lambda/\pi n_1$. This is also shown in Fig. 2.23.

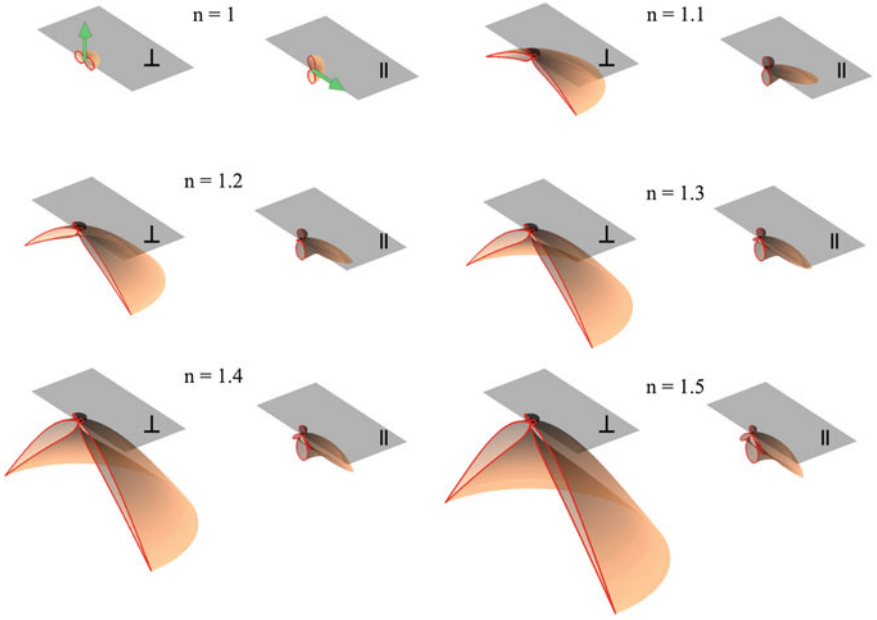

Fig. 2.20 Angular distribution of radiation power from a vertical and a paralle dipole located at the interface separating two dielectric media of refractive indices as shown above and below the dipole's position

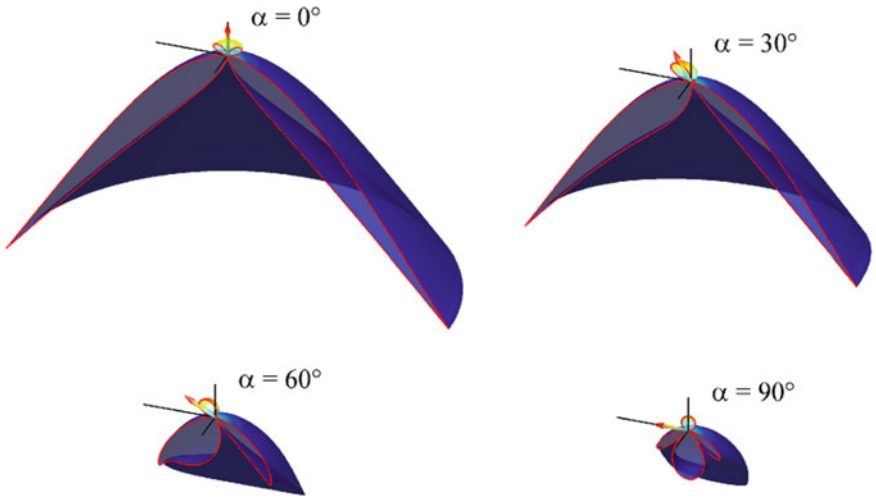

Fig. 2.21 Angular distribution of radiation of dipoles with various orientations on top of an air/glass interface. α denotes the angle between the dipole and the vertical direction

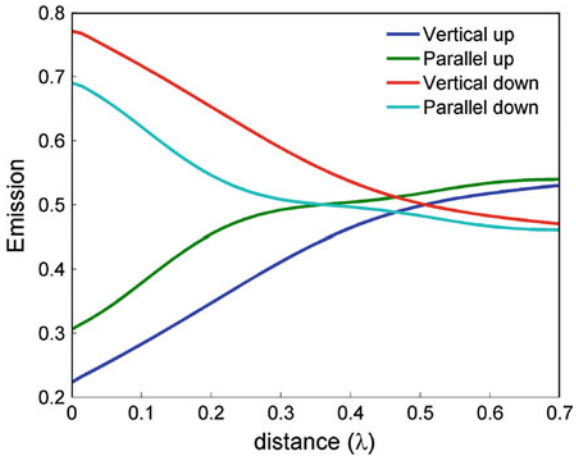

Fig. 2.22 Figure showing the distribution of power as a function of distance from a water/glass interface for a vertical and parallel dipole present in water. For a dipole situated at the interface, about 70% of total radiation power is transmitted into the glass half-space which shows the prominence of the effective near-field field coupling with the interface

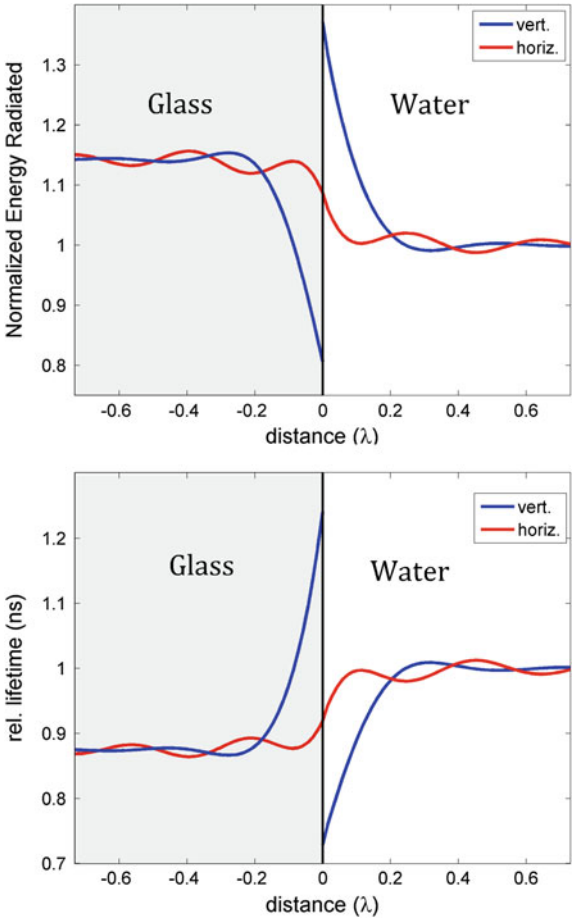

Fig. 2.23 The *top* figure shows the total energy radiated as a function of dipole's distance from the interface for both, vertical and parallel dipoles. The energy is normalized against the total radiation power of a dipole in an unbounded water medium. The oscillation amplitude of the curves goes to zero and the power converges to 1 (or 1.5/1.33) when the distance is on the order of a few wavelengths. The *bottom* figure shows the relative excited state lifetime as a function of distance from the interface normalized to the values in water

2.4.3 Dipole on a Metal Surface

Let us now investigate the behavior of a dipole in the vicinity of a metal surface. The properties of a dipole change dramatically in the vicinity of a metal surface. Due to the complex dielectric constant of a metal, a part of the electromagnetic radiation that is incident on them is absorbed. This absorption can be seen as a transfer of energy from the radiation to the oscillating plasmons on the surface. The situation is more complex when an oscillating dipole is present close to a metal. Not only does

a part of its radiated energy gets absorbed into the metal, but a near-field coupling between the dipole and the surface plasmons takes place. This changes the rate of energy emitted by the dipole dramatically. This is similar to what was presented in Sect. 2.4.2 for a dipole that is situated close to a dielectric interface in an optically rarer medium. There we saw that a few non-propagating modes of a dipole tunnel through and propagate in the optically denser medium. In case of metals, however, the energy that is transferred to the surface plasmons is attenuated along the z-direction. Therefore, the energy that is absorbed from the dipole's near-field is lost as heat in the metal internally and is not available for optical detection.

Several experimental studies have measured the effect of a metal surface on the fluorescence lifetime. During the early 70s, Drexhage and coworkers showed the influence of a reflecting mirror on a monolayer of phosphorescent europium chelate complexes experimentally, and developed a model to explain the variations in fluorescence lifetimes based on the interference of a dipole's field with itself [27]. This model could explain well the oscillatory behavior of the radiation rates at large distances from the metal surface, but failed to account for the experimental results at short distances ($z_0 < \lambda$) where efficient nonradiative energy transfer from the excited molecule to the metal surface takes place. At short distances, the europium complexes were quenched since the transferred energy was lost to the metal completely. The situation becomes slightly different for a thin metal film. The reduction of the thickness to a few nanometers leads to two things: 1) The coupling of the dipole's field with the surface plasmons present on the bottom side of the metal leading to a further modification of the distance-dependent energy loss. 2) Some part of the energy transferred to the metal can now propagate into the lower dielectric medium. This was demonstrated experimentally by Amos *et al.* by varying the thickness of a thin silver film on top of a glass coverslide [28].

A more appropriate theoretical treatment for studying the behavior of a dipole in the vicinity of a metal surface was performed by Kuhn in his model where the dipole is considered as a damped oscillator and involves the calculation of the reflected field at the dipole's position [29]. This way of calculating the total emission rates was already introduced in Sect. 2.4.1.1 using Poynting's theorem. Later, Chance, Prock and Silbey worked out the energy-flux method, which we will introduce briefly as well. With this model (CPS model) one can separate the total flux and radiation rates into the upper and lower half-spaces, useful for many practical purposes, such as calculating the amount of radiation from a dipole that can be detected through a thin film, etc [23]. The treatment is similar to that shown in the previous section where a dipole's reflected and transmitted fields are calculated when it is situated close to an interface and the total power radiated is calculated by integrating the Poynting vector for all the propagating waves in both half-spaces. However, here, in order to take the near-field coupling of a dipole with the metal surface into account, the integrals are calculated over all possible wave vectors, where q goes from 0 to ∞. We start our discussion by taking the transmitted and reflected fields of an oscillating dipole placed on top of an interface from our previous Sect. 2.4.2 using Fresnel's equations presented in the previous section.

$$\mathbf{E}_T(\mathbf{r}) = \frac{ik_0^2}{2\pi}\iint \frac{\mathrm{d}\mathbf{q}}{w_1}\left[\hat{\mathbf{e}}_{2p}^{+}T_p(\hat{\mathbf{e}}_{1p}^{+}\cdot\mathbf{p}) + \hat{\mathbf{e}}_s T_s(\hat{\mathbf{e}}_s\cdot\mathbf{p})\right] e^{i\left[\mathbf{q}\cdot(\boldsymbol{\rho}-\boldsymbol{\rho}_0)+w_1|z_0|+w_2 z\right]},$$

$$\mathbf{E}_R(\mathbf{r}) = \frac{ik_0^2}{2\pi}\iint \frac{\mathrm{d}\mathbf{q}}{w_1}\left[\hat{\mathbf{e}}_{1p}^{-}R_p(\hat{\mathbf{e}}_{1p}^{+}\cdot\mathbf{p}) + \hat{\mathbf{e}}_s R_s(\hat{\mathbf{e}}_s\cdot\mathbf{p})\right] e^{i\left[\mathbf{q}\cdot(\boldsymbol{\rho}-\boldsymbol{\rho}_0)+w_1|z_0|-w_1 z\right]}.$$

Here the reflection and transmission coefficients are complex numbers. The field in the upper half-space ($z < z_0$) can be written as a superposition of the dipole's field with its reflection from the interface

$$\begin{aligned}\mathbf{E}_{\uparrow} = \frac{ik_0^2}{2\pi}\iint \frac{\mathrm{d}\mathbf{q}}{w_1}\Bigg[&\hat{\mathbf{e}}_{1p}^{-}(\hat{\mathbf{e}}_{1p}^{+}\cdot\mathbf{p})\left(e^{-iw_1(z-z_0)} + R_p e^{-iw_1(z_0+z)}\right)\\ &+\hat{\mathbf{e}}_s(\hat{\mathbf{e}}_s\cdot\mathbf{p})\left(e^{-iw_1(z-z_0)} + R_s e^{-iw_1(z_0+z)}\right)\Bigg] e^{i\mathbf{q}\cdot(\boldsymbol{\rho}-\boldsymbol{\rho}_0)},\end{aligned} \tag{2.140}$$

and the field in the bottom half-space above the interface ($0 > z > z_0$) is given by

$$\begin{aligned}\mathbf{E}_{\downarrow} = \frac{ik_0^2}{2\pi}\iint \frac{\mathrm{d}\mathbf{q}}{w_1}\Bigg[&(\hat{\mathbf{e}}_{1p}^{+}\cdot\mathbf{p})\left(\hat{\mathbf{e}}_{1p}^{+}e^{-iw_1(z_0-z)} + \hat{\mathbf{e}}_{1p}^{-}R_p e^{-iw_1(z_0+z)}\right)\\ &+\hat{\mathbf{e}}_s(\hat{\mathbf{e}}_s\cdot\mathbf{p})\left(e^{-iw_1(z_0-z)} + R_s e^{-iw_1(z_0+z)}\right)\Bigg] e^{i\mathbf{q}\cdot(\boldsymbol{\rho}-\boldsymbol{\rho}_0)},\end{aligned} \tag{2.141}$$

The corresponding magnetic fields are obtained by performing the curl operation on the above equations followed by division by k_0

$$\begin{aligned}\mathbf{B}_{\uparrow} = \frac{ik_0^2 n_1}{2\pi}\iint \frac{\mathrm{d}\mathbf{q}}{w_1}\Bigg[&\hat{\mathbf{e}}_s(\hat{\mathbf{e}}_{1p}^{+}\cdot\mathbf{p})\left(e^{-iw_1(z-z_0)} + R_p e^{-iw_1(z_0+z)}\right)\\ &-\hat{\mathbf{e}}_{1p}^{-}(\hat{\mathbf{e}}_s\cdot\mathbf{p})\left(e^{-iw_1(z-z_0)} + R_s e^{-iw_1(z_0+z)}\right)\Bigg] e^{i\mathbf{q}\cdot(\boldsymbol{\rho}-\boldsymbol{\rho}_0)},\end{aligned} \tag{2.142}$$

$$\begin{aligned}\mathbf{B}_{\downarrow} = \frac{ik_0^2 n_1}{2\pi}\iint \frac{\mathrm{d}\mathbf{q}}{w_1}\Bigg[&\hat{\mathbf{e}}_s(\hat{\mathbf{e}}_{1p}^{+}\cdot\mathbf{p})\left(e^{-iw_1(z_0-z)} + R_p e^{-iw_1(z_0+z)}\right)\Bigg] e^{i\mathbf{q}\cdot(\boldsymbol{\rho}-\boldsymbol{\rho}_0)}\\ &-(\hat{\mathbf{e}}_s\cdot\mathbf{p})\left(\hat{\mathbf{e}}_{1p}^{+}e^{-iw_1(z_0-z)} + \hat{\mathbf{e}}_{1p}^{-}R_s e^{-iw_1(z_0+z)}\right),\end{aligned} \tag{2.143}$$

Using these equations, one can calculate the power radiated along any direction $(\boldsymbol{\rho}, z - z_0)$. Further, energy flux through any plane can be calculated by taking the dot product of the Poynting vector with the normal to this plane and integrating over the whole plane. In this way, the total flux through a plane above the dipole's position $z < z_0$ and below $0 \geq z > z_0$ can be calculated using the above four equations. Let us find out the total energy emitted into the lower half-space at the interface

($z = 0$). Using equations (2.141) and (2.143), one can write the Poynting vector $\mathbf{S}_\downarrow = c/8\pi \mathrm{Re}\{\mathbf{E}_\downarrow \times \mathbf{B}^*_\downarrow\}$

$$\mathbf{S}_\downarrow(\boldsymbol{\rho}, z=0) = \frac{ck_0^4}{32\pi^3}\mathrm{Re}\Bigg\{ \iint \frac{\mathrm{d}\mathbf{q}}{w_1} \iint \frac{\mathrm{d}\mathbf{q}'}{w_1'^* k_1} e^{i(\mathbf{q}-\mathbf{q}')\cdot(\boldsymbol{\rho}-\boldsymbol{\rho}_0)} \Bigg[\left(\hat{\mathbf{k}}_\mathbf{1}^{\ +} + R_p \hat{\mathbf{k}}_\mathbf{1}^{\ -}\right) e^{-iw_1 z_0} (e^{-iw_1' z_0})^* (1+R_p)^* (\hat{\mathbf{e}}_{1p}^{+} \cdot \mathbf{p})(\hat{\mathbf{e}}_{1p}^{+'} \cdot \mathbf{p})^* + \left(\hat{\mathbf{k}}_\mathbf{1}^{\ +} + R_s \hat{\mathbf{k}}_\mathbf{1}^{\ -}\right)^* e^{-iw_1 z_0} (e^{-iw_1' z_0})^* (1+R_s)(\hat{\mathbf{e}}_s \cdot \mathbf{p})(\hat{\mathbf{e}'}_s \cdot \mathbf{p})^* \Bigg] \Bigg\} \tag{2.144}$$

The above equation represents the energy flux at a point on the surface ($\boldsymbol{\rho}, z = 0$). By taking the projection of this vector along $\hat{\mathbf{z}}$, using the relations $\hat{\mathbf{z}} \cdot \hat{\mathbf{k}}_\mathbf{1}^{\pm} = \pm w_1/k_1$, and integrating over $\mathrm{d}^2\boldsymbol{\rho}$, we get the total radiation power through the interface $S_\downarrow = \int \mathrm{d}^2\boldsymbol{\rho}\,(\mathbf{S}_\downarrow \cdot \hat{\mathbf{z}})$. This integration can be simplified by using the identity of Dirac's well-known delta-function,

$$\int \mathrm{d}^2\boldsymbol{\rho} e^{[i\boldsymbol{\rho}\cdot(\mathbf{q}-\mathbf{q}')]} = 4\pi^2\delta^2(\mathbf{q}-\mathbf{q}'),$$

since the terms inside the square bracket in equation (2.144) do not depend on $\boldsymbol{\rho}$. This reduces equation (2.144) to

$$S_\downarrow = \frac{ck_0^4}{8\,\pi}\mathrm{Re}\Bigg\{ \iint \frac{\mathrm{d}\mathbf{q}}{|w_1|^2} \frac{qn_1^*}{k_1} \Bigg[w_1(1-R_p)(1+R_p^*) \left|\hat{\mathbf{e}}_{1p}^{+} \cdot \mathbf{p}\right|^2 + w_1^*(1+R_s)(1-R_s^*) \left|\hat{\mathbf{e}}_s \cdot \mathbf{p}\right|^2 \Bigg] e^{2\mathrm{Im}(w_1)z_0} \Bigg\} \tag{2.145}$$

Now, this equation represents the total energy flux at the interface and it contains the energy that is radiated from the dipole towards the interface together with the amount of energy reflected back. If a calculation was performed similarly at a plane above the dipole's position to give $S_\uparrow$, it would contain the dipole's radiation into the upper half space, together with the radiation reflected back as well. The total emission rate S can be calculated using equation (2.123) with the electric field at the position of the dipole calculated using either of the two equations (2.141) or (2.140) [30, 31].

Let us now consider closely the case of a vertical dipole, $\mathbf{p} = p\hat{\mathbf{z}}$. The integration over $\mathbf{q}$ can be carried out in spherical coordinates

$$S_{\perp\downarrow} = \frac{ck_0^4 p^2}{4}\mathrm{Re}\Bigg\{ \int \frac{\mathrm{d}q}{|k_1 w_1|^2} \frac{q^3 n_1^* w_1}{k_1} (1-R_p)(1+R_p^*) e^{2\mathrm{Im}(w_1)z_0} \Bigg\} \tag{2.146}$$

Using (2.140) and after some algebraic manipulations, the total radiation power $S_\perp$ is obtained as

$$S_{\perp} = \frac{ck_0^4 p^2}{2}\mathrm{Re}\left\{\int \frac{\mathrm{d}q}{|k_1 w_1|^2}\frac{q^3 n_1^* w_1}{k_1}(1 + R_p e^{-2iw_1 z_0})\right\} \tag{2.147}$$

Similarly, for a parallel dipole, one has

$$S_{\parallel\downarrow} = \frac{ck_0^4 p^2}{8}\mathrm{Re}\left\{\int \frac{\mathrm{d}q}{|w_1|^2}\frac{qn_1^*}{k_1}\right. \tag{2.148}$$
$$\left.\left[\frac{|w_1^2|}{k_1^2}w_1(1 - R_p)(1 + R_p^*) + w_1^*(1 + R_s)(1 - R_s^*)\right]e^{2\mathrm{Im}(w_1)z_0}\right\}$$

and the total radiation power,

$$S_{\parallel} = \frac{ck_0^4 p^2}{4}\mathrm{Re}\left\{\int \frac{\mathrm{d}q}{|w_1|^2}\frac{qn_1^* w_1}{k_1}\left[\frac{|w_1^2|}{k_1^2}(1 + R_p e^{-2iw_1 z_0}) + (1 + R_s e^{-2iw_1 z_0})\right]\right\} \tag{2.149}$$

All the integrals above were performed for all possible q (0 to ∞) values together with positive imaginary solutions of $w_1(q)$ only. This gives the total power emitted by the dipole into both the half-spaces $S_{\uparrow}$ and $S_{\downarrow}$. In order to calculate the rate of energy *detectable* in both the half-spaces, one limits the upper-limit of the integrals to propagating wave vectors only. An important point to note here is that for the integrals (2.146) and (2.148) when $q < k_1$, $\mathrm{Im}(w_1) = 0$, and therefore the integrals do not depend on the dipole's position. These then represent the "trivial transfer" of radiation power to the metal surface from the far-field of the dipole [23]. In other words, this shows the fraction of energy that is absorbed by the metal.

In order to complete the discussion here and to make use of what we just derived, we calculate the total power that is *detectable* in both half-spaces for the two cases of dipole orientations for a thin metal film on top of a glass coverslip. We do this by calculating the ratio of the net propagating part of the radiation power to the total power in both half-spaces. The above equations are true for such a stratified conducting/dielectric layer system, as long as one uses the effective reflection coefficients [24]. For a thin metal film sandwiched between glass and air, one has:

$$R_{p,s} = \frac{r_{p,s}^{12} + r_{p,s}^{23}\exp(2iw_2 h)}{1 + r_{p,s}^{12} r_{p,s}^{23}\exp(2iw_2 h)} \tag{2.150}$$

where the subscripts refer to p- and s-polarization, $r_{p,s}^{12}$ and $r_{p,s}^{23}$ are the Fresnel reflection coefficients for an air-to-metal and metal-to-glass interface, and $w_2 = \sqrt{(n_2^2 - 1)k_0^2 + w_1^2}$, where n_2 is the complex refractive index of metal.

Figure 2.24 shows the energy emitted that is detectable as a function of height. The quantum yield for the dipoles was assumed to be one. Note that at distances $z_0 > \lambda$, the total radiated energy into both half-spaces approach constant values that represent the net reflectance and transmittance of the metal film. Two important things should

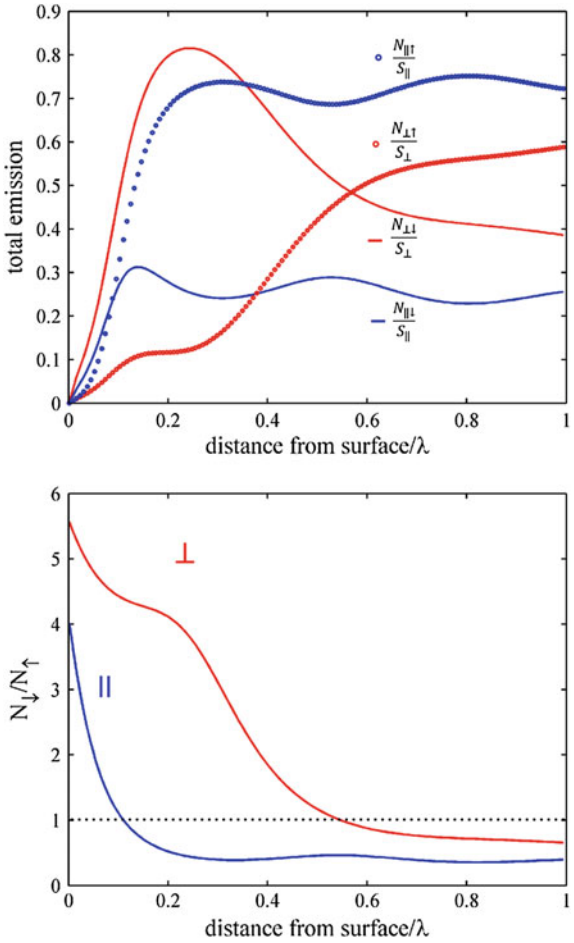

Fig. 2.24 $N_\uparrow, N_\downarrow$ represent the detectable energy calculated for both the upper and lower half-spaces, respectively. The *top* figure shows the detectable radiation of a dipole ($\Phi = 1$) into the upper and lower half-spaces for both orientations as a function of distance d ($d = z_0/\lambda,\ \lambda = 690\,\text{nm}$). The thin gold film of 10 nm is enough to quench the dipoles. This can be seen in the plot where the radiation in the upper and lower half-spaces approach zero when the dipole is placed at very small distances. A part of the energy that is transferred to the surface plasmons couples out at the gold/glass interface which propagates into the lower half-space. The *bottom* figure shows the ratio of the detectable emission power in the lower half-space versus the upper half-space for both the orientations as a function of distance from the metal surface. This shows that when a dipole is close to the surface of a thin film, the chance to detect it optically is higher through the glass beneath

be noted from this figure. First, the thin gold film of thickness 10 nm is enough to quench the dipoles in its vicinity. In other words, the plasmons excited due to the transfer of energy from the dipole radiate out in the bottom interface between gold and glass medium. In other words, a part of the energy transferred to the plasmons from the oscillating dipole close to it is transferred further into the glass medium where it can propagate again. This energy now propagates in the form of plane waves and can be detected by our optical system with a high collection efficiency objective. The possibility to detect single molecules on top of a thin metal film, with some spacer in between, was first shown by Stefani *et al.* [32].

Dividing equation (2.147) by the total radiation power of a free dipole in the same medium ($n_1 S_0 = c n_1 k_0^4 p^2/3$), we get rate associated with the total photon flux from a dipole close to a metal surface

$$\kappa_\perp = \kappa_0 \left[1 - \frac{3}{2} \mathrm{Re} \left\{ \int_0^\infty \frac{\mathrm{d}u}{w_1} u^3 R_p e^{-2i w_1 z_0} \right\} \right], \tag{2.151}$$

where we used $u = q/k_1$ in the above equation, and κ_0 is the radiative rate of a free dipole (see equation (2.126)). On similar lines, the total photon flux of a parallel dipole can be obtained

$$\kappa_\parallel = \kappa_0 \left[1 + \frac{3}{4} \mathrm{Re} \left\{ \int_0^\infty \frac{\mathrm{d}u}{w_1} u \left[R_s + (1 - u^2) R_p \right] e^{-2i w_1 z_0} \right\} \right]. \tag{2.152}$$

If the quantum yield ϕ of the free dipole is not unity, then the total rate of photons for a vertical dipole can be separated into the sum of a radiative ($\kappa_{r\perp}$) and a non-radiative decay rate ($\kappa_{nr\perp}$) as

$$\kappa_{r\perp} = \kappa_0 \left[\Phi - \frac{3}{2} \Phi \, \mathrm{Re} \left\{ \int_0^1 \frac{\mathrm{d}u}{w_1} u^3 \left(R_p \right) e^{-2i w_1 z_0} \right\} \right] \tag{2.153}$$

and

$$\kappa_{nr\perp} = \kappa_0 \left[(1 - \Phi) - \frac{3}{2} \Phi \, \mathrm{Re} \left\{ \int_1^\infty \frac{\mathrm{d}u}{w_1} u^3 \left(R_p \right) e^{-2i w_1 z_0} \right\} \right]. \tag{2.154}$$

The above equations are trivial to understand. w_1 is real only when u varies from $0 \rightarrow 1$. Since the radiative rate is associated with propagating plane waves originating from the dipole, the integral takes into account only these values of u. The factor $\kappa_0(1 - \Phi)$ is the intrinsic non-radiative damping constant of the oscillator and it represents the fraction of energy that is not available for any energy transfer or emission processes. The effect of the metal or the local environment on the dipole is realized on the radiative part of the energy which is given by $\kappa_0 \Phi$. Due to the presence of a metal surface here, a part of this radiative energy appears as non-radiative energy which is accounted for by the integral term in expression (2.154). Therefore, this integral represents the metal-induced energy transfer.

$$\kappa_{\mathrm{MIET}\perp} = \frac{3}{2}\kappa_0 \Phi \,\mathrm{Re}\left\{\int_1^\infty R_p e^{-2iw_1|z_0|} u^3 \frac{\mathrm{d}u}{w_1}\right\} \tag{2.155}$$

At distances on the order of a wavelength and closer to the metal surface, both the radiative as well as the non-radiative rates are modified as according to equations (2.153) and (2.154), respectively. One more important thing to note here is that the extent of energy transfer to the metal is directly related to the quantum yield Φ of the dye molecules. Therefore, one is bound to know the exact quantum yield in order to estimate the total radiative rate and fluorescence lifetime as a function of distance. Figure 2.25 shows the variation of lifetimes with distance for the two orientations of a dipole with various quantum yields. An important observation here is that at any height $|z_0|$ above the surface, the energy transfer scales proportionally with the quantum yield of the dye, as represented by Eq. (2.155). Therefore, if the free space lifetimes of two fluorescent molecules, with different quantum yields, are identical, then at a given distance from a metal surface, lifetime of the molecule with higher quantum yield is shorter.

For a dipole oriented at an angle α with respect to the normal of the surface, one can derive the total emission power $S(\alpha, z_0)$, using the reflected electric field from equation (2.130), together with its own field, and equation (2.123) (Poynting's Theorem) in terms of the total emission power of a vertical and parallel dipole. If the quantum yield of the dipole is Φ, then the rate of excited state decay can be written by dividing the total emission power by $n_1 S_0$ (radiation power of a free dipole in the same medium)

$$\kappa(\alpha, z_0) = \kappa_0 \left[(1-\Phi) + \Phi \frac{S(\alpha, z_0)}{n_1 S_0}\right] = \frac{1}{\tau_f(\alpha, z_0)} \tag{2.156}$$

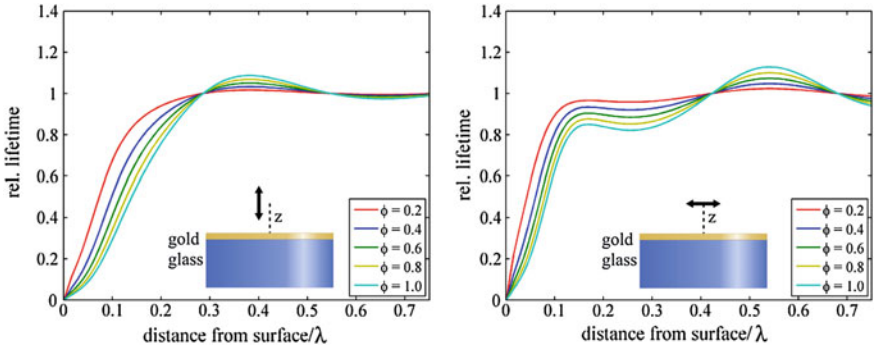

Fig. 2.25 The *Left* figure shows the relative lifetime variation with the distance from a 10 nm gold film for a vertical dipole with various quantum yield. The *right* figure shows the same for a parallel dipole

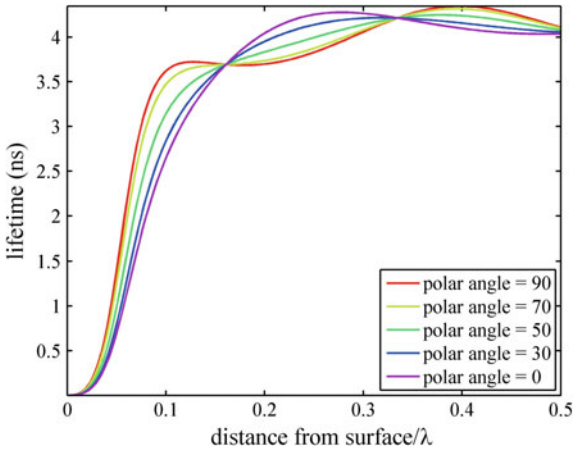

Fig. 2.26 MIET calibration curves of Rhodamine 6G in water on top of a thin gold film at various polar angles. The calculations were done for a thin gold film of thickness $h = 10$ nm, with water as a medium above at a wavelength $\lambda_{em} = 525$ nm. The free space parameters for the dye are taken from the reference [19]

Fig. 2.26 shows the MIET calibration curves of Rhodamine 6G ($\tau_0 = 1/\kappa_0 = 4.1$ ns and $\Phi = 0.95$, see reference [19]) for five different dipole orientations with water as a medium above a thin gold film (h=10 nm) at an emission wavelength $\lambda_{em} = 525$ nm.

Regardless of its quantum yield and orientation α, the excited state lifetime of a single molecule shows a monotonic relationship with distance from the metal surface in the near-field limit, and therefore, can be used to locate the emitter from the surface. This is much similar to FRET where the energy is transferred non-radiatively to another dipole. However, the distance to lifetime relationship in the case of FRET shows an inverse sixth power relationship ($\Delta\tau/\tau_0 \propto d^{-6}$), whereas in the case of an infinite plane of a metal surface, it is roughly proportional to d^{-3} to d^{-4} [23].

This concludes the theory to explain the concept of metal-induced energy transfer completely. The emission properties of an electric dipole emitter in the presence of a dielectric or metallic interface are calculated by expressing its electric field as a superposition of plane waves, and thereafter calculating the reflected and transmitted fields by using Fresnel's equations. The modified spontaneous emission rate is then obtained directly by calculating the reflected field at its position and applying Poynting's theorem (2.122). Energy flux calculations by estimating the Poynting vector allows one to separate the total energy radiated into both half-spaces, and further, to picture the angular distribution of emission. This includes the involvement of various processes which have not been precisely named in this chapter such as Surface Plasmon Coupled Emission (SPCE), Surface Plasmon Resonance (SPR), Lossy Surface Waves (LSW), Radiating Plasmons (RP), etc [33–35]. Introducing these terms and terminology is confusing and is not required in order to explain the necessary emission properties of a single molecule near a metal surface or a thin metal film. The theory above is in fact completely identical to the theoretical work of Purcell

who derived the spontaneous emission probabilities of nuclear transitions in metallic resonators. The idea is based on the enhancement of the local density of final states in, for example, a cavity or near a conducting surface.

References

1. I.N. Levine, P. Learning, *Quantum Chemistry*, vol. 6 (Pearson Prentice Hall, Upper Saddle River, NJ, 2009)
2. P. Atkins, R.S. Friedman, *Molecular Quantum Mechanics*, (Oxford University Press, 2011)
3. N. Obi-Egbedi, I. Obot, Arab. J. Chem. **5**, 121 (2012)
4. A. Penzkofer, J. Wiedmann, Opt. Commun. **35**, 81 (1980)
5. L. Cavallo, M.H. Moore, J.E. Corrie, F. Fraternali, J. Phys. Chem. A **108**, 7744 (2004)
6. M. Kasha, *Radiation Research Supplement Sbf*, p. 243 (1960)
7. E. Clementi, M. Kasha, J. Mol. Spectrosc. **2**, 297 (1958)
8. A. Boguta, D. Wróbel, J. Fluoresc. **11**, 129 (2001)
9. R. Englman, J. Jortner, Mol. Phys. **18**, 145 (1970)
10. M. Bixon, J. Jortner, J. Chem. Phys. **48**, 715 (1968)
11. M. Bixon, J. Jortner, J. Chem. Phys. **50**, 3284 (1969)
12. E.M. Purcell, Phys. Rev. **69**, 681 (1946)
13. P.A. Dirac, in *Proceedings of the Royal Society of London A: Mathematical, Physical and Engineering Sciences*, vol. 114 (The Royal Society, 1927)
14. R. Ladenbarg, Zeitschrift für Physik A **4**, 451 (1921)
15. W.L. Barnes, R. Laming, E.J. Tarbox, P. Morkel, IEEE J. Quantum Electron. **27**, 1004 (1991)
16. R.C. Tolman, Phys. Rev. **23**, 693 (1924)
17. S. Strickler, R.A. Berg, J. Chem. Phys. **37**, 814 (1962)
18. J.M. Dixon, M. Taniguchi, J.S. Lindsey, Photochem. Photobiol. **81**, 212 (2005)
19. N. Karedla, J. Enderlein, I. Gregor, A.I. Chizhik, J. Phys. Chem. Lett. **5**, 1198 (2014)
20. S. Lin, S. Lee, Y. Yoon, H. Eyring, Proc. Natl. Acad. Sci. **73**, 2533 (1976)
21. K. Joulain, R. Carminati, J.-P. Mulet, J.-J. Greffet, Phys. Rev. B **68**, 245405 (2003)
22. P. Anger, P. Bharadwaj, L. Novotny, Phys. Rev. Lett. **96**, 113002 (2006)
23. R. Chance, A. Prock, R. Silbey, Adv. Chem. Phys **37**, 65 (1978)
24. M. Born, *Principles of Optics: Electromagnetic Theory of Propagation* (Interference and Diffraction of Light, CUP Archive, 2000)
25. I.V. Ahlfors, *Complex Analysis: An Introduction to the Theory of Analytic Functions of One Complex Variable* (1979)
26. D.J. Griffiths, R. College, *Introduction to Electrodynamics*, vol. 3 (Prentice Hall, Upper Saddle River, NJ, 1999)
27. K.H. Drexhage, *Progress in Optics* , p. 163 (1974)
28. R. Amos, W. Barnes, Phys. Rev. B **55**, 7249 (1997)
29. H. Kuhn, J. Chem. Phys. **53**, 101 (1970)
30. J. Enderlein, Biophys. J. **78**, 2151 (2000)
31. J. Enderlein, Chem. Phys. **247**, 1 (1999)
32. F. Stefani, K. Vasilev, N. Bocchio, N. Stoyanova, M. Kreiter, Phys. Rev. Lett. **94**, 023005 (2005)
33. J.R. Lakowicz, Anal. Biochem. **337**, 171 (2005)
34. J.R. Lakowicz, Anal. Biochem. **324**, 153 (2004)
35. G.W. Ford, W.H. Weber, Phys. Rep. **113**, 195 (1984)

http://www.springer.com/978-3-319-60536-4

Single-Molecule Metal-Induced Energy Transfer
From Basics to Applications
Karedla, N.
2017, XVIII, 166 p. 96 illus., 34 illus. in color., Hardcover
ISBN: 978-3-319-60536-4